VIBRATION OF TURBINE BLADES BY FINITE ELEMENT METHOD

by

AJIT B. EKBOTE

DEPARTMENT OF MECHANICAL ENGINEERING

INDIAN INSTITUTE OF TECHNOLOGY, KANPUR

MAY, 1987

VIBRATION OF TURBINE BLADES BY FINITE ELEMENT METHOD

A Thesis Submitted
In Partial Fulfilment of the Requirements
for the Degree of
MASTER OF TECHNOLOGY

by

AJIT B. EKBOTE

to the

DEPARTMENT OF MECHANICAL ENGINEERING
INDIAN INSTITUTE OF TECHNOLOGY, KANPUR
MAY, 1987

To

my parents

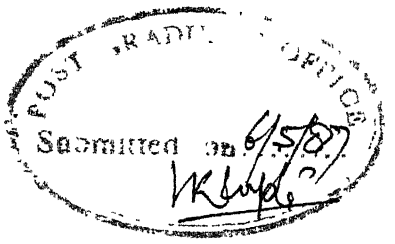

CERTIFICATE

This is to certify that the work entitled "Vibrations of Turbine Blade by Finite Element Method" by Ajit B. Ekbote has been carried out under our supervision and has not been submitted elsewhere for a degree.

Dr. P. M. Dixit
Assistant Professor
Dept. of Mech. Engg.
I. I. T., Kanpur

Dr. B. L. Dhoopar
Professor
Dept. of Mech. Engg.
I. I. T., Kanpur

May, 1987

ACKNOWLEDGEMENTS

I express my sincere thanks to my thesis supervisors, Dr. B.L. Dhoopar and Dr. P.M. Dixit, for their able and invaluable guidance and for devoting their precious time to solve my difficulties.

I am profoundly grateful to Dr. T. Sundararajan for his invaluable help in the nick of time, when I was stuck with a computational problem.

I express my thanks to Dr. B.P. Singh for making available some literature.

Love and sincerity of my fellow students and all my friends made my sojourn here an enjoyable experience.

I express my thanks to Mr. R.N. Srivastava for careful typing of my manuscript and Mr. A.K. Pradhan for his neat tracings.

- Ajit

TABLE OF CONTENTS

LIST OF TABLES

LIST OF FIGURES

NOTATIONS AND SYMBOLS

A	area of cross-section
$\underline{\underline{A}}_b$	tensor relating the reference area moments of inertia to the principal area moments of inertia
$\underline{\underline{A}}_1$, $\underline{\underline{A}}_2$	tensors
a	half the element size for two noded beam element
$\underline{\underline{B}}$	a tensor in the governing equation
b	breadth of rectangular section, chord length of aerofoil section
C	torsional stiffness
$\underline{\underline{C}}$	a tensor in the governing equation
C_1	St. Venant torsional stiffness
C_2	stiffness due to fibre-bending
C_3	stiffness due to pre-twist.
D	flexural rigidity of the plate
E	Young's modulus
e	Napierian base, suffix indicating element, eccentricity in the Zukovsky transformation
$f(x,y)$	function of x and y
$f(z)$	function of z
G	modulus of rigidity
h	thickness of rectangular cross-section, maximum thickness of aerofoil section
$\underline{\underline{I}}$	inertia tensor
I_{av}	average area moment of inertia

I_{cf}	area polar moment of inertia about flexural centre of the cross-section
I_{cm}	area polar moment of inertia about centroid of the cross-section
I_{mu}	average difference in the area moments of inerti
I_{xx}, I_{yy}	area moments of inertia about the reference axes
I_{xy}	area product of inertia about the reference axes
I_{11}, I_{22}	principal area moments of inertia
i	-1, suffix
$\underline{\underline{K}}$	global stiffness matrix
$\underline{\underline{K}}^e$	element stiffness matrix
l	length of the plate as well as beam
$\underline{\underline{M}}$	global mass matrix
$\underline{\underline{M}}^e$	element mass matrix
$\underline{\underline{M}}_m$	moment tensor
M_x, M_y, M_{xy}	stress resultants for plate
$\hat{n}$	unit outward normal to the boundary
ngx, ngy	number of Gauss points along x and y direction respectively
P_i	shape function
p	half the length of the element
$\underline{Q}$	shear force vector
Q_j	shape function
q	half the breadth of the element, x coordinate of the centre of circle in Zukovsky transformation
$\underline{R}^e$	element stress-resultant vector

r_x, r_y	coordinate distances between the centroid and the flexural centre
$\underline{\underline{S}}$	shape function tensor
T	kinetic energy
t	time
$\underline{U}^e$	element displacement amplitude vector
U_i	amplitude of flapwise displacement at the i^{th} no of an element
u	flapwise bending deflection
$\underline{u}$	displacement vector at a point
u_i	flapwise displacement at the i^{th} node of an elem
V	potential energy
V_i	amplitude of chordwise displacement at the i^{th} node of an element
v	chordwise bending deflection
v_i	chordwise displacement at the i^{th} node of an elem
W_1, W_2, W_3, W_4	amplitude of displacements at the nodes
$\underline{W}^e$	nodal displacement vector
w	displacement of a point on the middle surface along z-axis
w_i, w_j	weight functions corresponding to Gauss points x_i
xx	reference coordinate
x_c	global coordinate of mid-point of an element
x_e	global coordinates of e^{th} node of an element
yy	reference coordinates
y_c	global coordinate of mid-point of element
y_e	global coordinates of e^{th} node

z	spatial coordinate, complex number
zz	reference coordinates
z_c	global coordinate of mid-point of element
z_e	global coordinates of e^{th} node of an element

Greek symbols:

β	angle in the Zukovsky transformation
γ	pre-twist
δ	variation
ε^e	residue over the element
ζ	complex number
η	natural coordinate of the element, imaginary part of
η_i	local coordinate of the node
Θ_i	amplitude of the torsional displacement at the i^{th} node of an element
θ	torsional deflection, polar coordinate
λ	eigen-value
μ	Poisson's ratio, eigen-value
ξ	natural coordinate of the element, real part of
ξ_i	local coordinate of the node
ρ	density
Σ	summation
σ_{xx}, σ_{yy}, σ_{xy}	significant components of the stress tensor
ϕ	shape function
ω	frequency
ω_o	non-dimensionalised frequency

Notations:

d	total differentiation
$\cdot$	partial differentiation with respect to time t
$'$	partial differentiation with respect to spatial coordinate z
$\int$	integration
∂	partial differential operator
∇	directional derivative
∇^2	Laplacian

ABSTRACT

The investigation of the vibrations of a turbine blade has been a fascinating and challenging problem to the design engineers and the research workers and they have

i) idealized it as a beam, a plate and a shell,

ii) incorporated one after another the additional effects of asymmetry of the cross-section, taper, pre-twist, stagger camber, packetting, rotary inertia, shear deformation etc. and

iii) utilized different approximate/numerical techniques of solution like Rayleigh-Ritz, Ritz-Galerkin, Holzer, Collocation, FDM, FEM etc.

Here, the free vibration of a stationary blade has been dealt with modelling it as a beam and as a plate. The finite element technique using Galerkin's method has been employed to reduce the system of partial differential equations to a matrix eigen-value problem. The eigen-values and the eigen-vectors were computed using a NAG subroutine F02AEF which makes use of the Householder's decomposition and the QL algorithm. As the first eigen-value, thus computed, exhibited oscillating trend rather than converging to its lower bound with the increase in the number of elements, in lieu of the eigen-value problem, an inverse eigen-value problem was solved.

To determine whether a blade of asymmetric cross-section can be treated as a beam, one needs to compute the chord length and the maximum thickness of the cross-section. This has been done invoking Zukovsky's transformation. While treating the blade as a beam, the asymmetry of the cross-section and the pre-twist accompanied by the fibre-bending during torsion were accounted for. The frequencies were computed for three different data of the blade. The effect of pretwist on the coupled bending-bending modes and the torsional modes for a beam of a rectangular cross-section was studied. When treated as a plate, the blade was assumed to be so thin that the effect of the rotary inertia and the shear deformation could be neglected. In computation of the element stiffness matrix and the element mass matrix, integration was carried out by a Gauss quadrature formula. The frequencies were computed for four different aspect ratios of the blade. All the results obtained were compared with those obtained by the respective authors.

CHAPTER 1

INTRODUCTION

The turbomachines are widely used in the steam turbines, gas turbines, compressor and gas turbines of the aircraft propulsion systems, marine drives etc. The steam turbines comprise of three stages called as high pressure (HP), intermediate pressure (IP) and low pressure (LP); each stage consists of the moving blades fixed to the rotor and the stationary blades fixed to the casing. The turbine blades are the soul of the whole turbomachine. The minimum satisfactory height of impulse blading is from 0.1 to 2.5 cm in small turbines and from 4.0 to 5.0 cm in large turbines [23]. The values of exit angle for the turbine blades in vogue vary from 150° to 165° at HP and IP stages and from 140° to 150° at the LP stage, sometimes reaching 130° to 140° in the final stage of large turbines where maximum flow is needed. The values of the chord length of the bladings of the impulse turbine range from 4.0 to 5.0 cm at the HP end to 15 cm or more at the LP end. The HP turbine blades are short, and tapered, have nearly equal entrance and exit angles thus requiring small angle of the pre-twist — say of the order of 2°, have stagger angle between 25° to 35°, and are banded at a definite pitch. The LP turbine blades are long with considerable pre-twist. In general, a turbomachine blade is a tapered, pre-twisted, staggered and cambered cantilever of asymmetric airofoil cross-section.

Because of asymmetry, the centroid and the flexural centre of the aerofoil section do not coincide.

The working fluid, throttled through a nozzle, flows over a blade and in due course exerts a tangential force on it, thereby causing it to rotate about the turbine axis and to undergo bending and torsional deformation. The process of power generation in the turbine leads to the excitation of the blades because of the flow pattern of the working fluid. Cyclic stresses are set in the blades due to forced vibrations. They are detrimental to the blades as they are likely to cause fatigue failure. Moreover, if the forcing frequency is close to the natural frequency of the blade, it leads to the phenomenon of resonance thus further enhancing the amplitude of cyclic stresses and hence increasing the probability of fatigue failure of the blade. Therefore, it is imperative to know the natural frequencies of the turbine blade.

The vibration analysis of the turbine blades has been evolved from using the simple beam theory to that of the sophisticated finite element techniques. When idealised as a simple cantilever beam of symmetric cross-section (rectangular), the analysis of vibrations of the blade is quite simple. The analysis of the blades with aerofoil section has been arrived at, incorporating successively the effects of taper, asymmetry, pre-twist, fibre-bending, Coriolis force, centrifugal force, stagger angle, rotary inertia and shear deformation. Additional effects due to factors like residual stresses, relief of

stresses of cambered section during bending, the penetration of the stress pattern into the root, the angle at the root and tip to the axis of the blade, non-coincident flexural and torsional centres etc. have been studied by various researchers. Modelling the blade as a cantilever beam with asymmetric aerofoil section, pre-twist and taper can give good results when the length of the blade is much greater than the other dimensions. However, a short flat blade has to be idealized as a thin plate and a short twisted blade a thin shell. The effects of rotary inertia and shear deformation have also been incorporated and studied by many researchers and scientists [13], [15], [17].

When idealized as a uniform straight beam of asymmetric aerofoil section, the blade exhibits the coupled vibrations of flap-wise bending, chord-wise bending and torsion. This is owing to the asymmetry of the section by virtue of which the centroid and the flexural centre are non-coincident whereas when considered as a beam of rectangular cross-section (the centroid and the flexural centre being coincident) coupled bending-bending vibrations occur which are attributed to the pre-twist. Because of pre-twist the product of inertia comes into picture which couples the flap-wise bending and chord-wise bending; but the torsion remains uncoupled. The only factor to couple torsional modes to the bending modes is distinct location of centroid and flexural centre. If the blade is assumed to behave as a flat rectangular cantilever plate, no coupling occurs between bending and torsional modes,

as the displacements along the axis and the chord are directly proportional to the slopes along the axis and the chord respectively. Nevertheless, in the case of the plate also, coupling occurs only if it is pre-twisted in which the two dimensional element has to be treated as a shell. In all the cases discussed above, it is difficult to obtain the closed form solution. Hence one has to resort to the approximate/ numerical methods like Rayleigh-Ritz, Holzer, Collocation, Galerkin, FDM, FEM etc.

BRIEF REVIEW OF THE AVAILABLE LITERATURE:

Houbolt and Brooks [1] developed the differential equations of motion for the lateral and torsional deformations of twisted rotating beams without the loss of generality as regards the non-coincidence of the torsional, flexural and centroidal axes for the application to helicopter rotor and propeller blades. Carnegie [2] derived the governing equations of coupled bending-bending-torsion motion of thin pre-twisted cantilever blade using variational method. He incorporated the additional effect due to pre-twist while studying the vibrations of a straight, pre-twisted uniform blade of rectangular cross-section as a special case. Paranjpe [3] studied the self-sustained oscillations of the turbomachine blading which were likely to occur particularly when light sections were subjected to heavy aerodynamic loading. Carnegie [4] derived the general equations of motion of the rotating cantilever blade applying the variational method. Kulkarni et al [15]

applied both the Reisner method and the total potential energy approaches to deduce the equations of the coupled bending-bending vibrations of the pre-twisted uniform rectangular cantilever blade accounting for the shear-deformation and the rotary inertia effect. They found out the natural frequencies by Ritz process and compared these with the experimental results for a specific data.

Duggan and Slyper [5] applied a modified central finite difference method to the equations of motion to compute the natural torsional frequencies of vibration of the pre-twisted cantilever beams of non-uniform symmetric cross-section considering the effect of fibre-bending. Belgaumkar et al [6] obtained the natural frequencies of the torsional vibration of a cantilever beam of rectangular cross-section with uniform taper by collocation method and compared these with those determined by Holzer's method [6]. Carnegie and Rao [7] applied Galerkin's procedure to determine the natural frequencies of an untwisted cantilever blade with an asymmetric aerofoil cross-section executing coupled bending-bending-torsion vibrations, neglecting the effect of the fibre-bending. Rao [8] computed the coupled bending-bending frequencies of a pre-twisted cantilever blade of the uniform rectangular cross-section. He [9] determined the coupled bending-bending-torsion frequencies of vibrations of a uniform untwisted cantilever beam of an asymmetric aerofoil section using the collocation method and ignoring the effect of the fibre-bending. He [10] computed the natural frequencies of the

torsional vibrations of a pre-twisted cantilever beam with the uniform rectangular cross-section.

Carnegie and Rao [11] found out the natural frequencies of the torsional vibrations of the tapered, pre-twisted cantilever beams of the rectangular cross-section. Gupta and Rao S.S. [13] used finite element method (FEM) to study the vibration of a single, tapered, pre-twisted blade of an aerofoil cross-section. Bajaj and Dhoopar [14] studied the vibrations of the packetted, tapered blade of the rectangular cross-section with the negligible pre-twist applying FEM. Kaza and Subrahmanyam [16] solved the problem of calculating the natural frequencies and the mode shapes of the rotating blades by a finite difference method (FDM). Saurabh Kumar [18] tackled the problem of the coupled bending-bending-torsional vibrations of a single cantilever blade with the effects of the pre-twist, rotation, hub-radius, stagger angle and the asymmetry of the cross-section by FEM using the Galerkin's technique. Rao [12] compiled the results pertaining to the effects of the speed of rotation, asymmetry, stagger angle and hub radius on the natural frequencies of the vibrations of the pre-twisted cantilever bladings used for the turbo-machines.

In their state of art paper, Leissa, Kielb and Macbain [17] compiled the results of vibration of the twisted cantilever plate obtained by a joint government/industry/university research study. The numerical results were obtained for twenty different geometries using nineteen different methods —

15 using FEM, 2 using shell theory, 2 using beam theory — in order to have comprehensive, definitive set of results. The graph of the non-dimensionalised frequency versus the pre-twist exhibited different trends in some cases, so much so, that the predicted dependency of the frequency on the twist-angle for the twisted cantilever plates spanned the spectrum from increasing significantly to decreasing significantly. This, indeed, made the problem quite challenging and fascinating.

SCOPE OF THE PRESENT WORK:

The present work aims at studying the free vibration of the turbine blade treating it as a) a beam and b) a plate by finite element method (FEM). It is observed that the effect of rotation of the blade is negligible, hence we study the vibrations of non-rotating blades. To limit the study to a manageable size, the effects of stagger, camber, taper, centrifugal force, Coriolis force, rotary inertia, shear deformation, packetting, hub-radius etc. are neglected.

As reviewed above, vibrations of the blade treating it as a beam have been analysed by various authors using classical approximate methods. The objective of this work is to re-analyse some of these problems using FEM thereby establishing that FEM can be used sufficiently accurately to obtain the natural frequencies of straight or pre-twisted long blades by treating it as a beam. FEM has been used by some authors earlier also but not so extensively. It is also established that a short straight blade has to be analysed as a plate and here also FEM can be

used with reasonable accuracy. A short twisted blade has to be modelled as a shell. Due to lack of time, this study could not be undertaken.

Chapter 2 deals with the problem of vibration of a blade considering it to be:

1) straight, untwisted beam of asymmetric aerofoil section in coupled bending-bending-torsional modes caused due to the asymmetry of the section. The data used in the reference [12] to solve the problem is used to compute numerical values of the natural frequencies and to compare the results with those obtained in the same paper. Coupled modes of a straight cantilever blade are studied assuming that the principal axes of the aerofoil section are closely located to the reference axes, say of the order of 2°. In other words, the product of inertia with respect to the reference axes is assumed to be negligible. The effect of fibre-bending is ignored in this case.

2) Straight beam of rectangular cross-section — untwisted as well as pre-twisted. For untwisted blade, flapwise bending, chordwise bending and torsion are all uncoupled. In the case of pre-twisted beam, flapwise and chordwise bendings get coupled due to pre-twist but torsion remains uncoupled as centroid and shear-centre of the section are the same. Using the data of the references [18] and [8] and incorporating the effects of pre-twist and fibre-bending, the results are obtained by FEM and compared with those given in the same paper. Using the data of the reference [17] and ignoring the effect of fibre-bending, the natural

frequencies are computed and the results are compared with those compiled in this paper.

Chapter 3 consists of modelling the blade as a simple cantilever uniform thin plate of rectangular cross-section. The flapwise bending, chordwise bending and torsion are not coupled because displacements along axis and chord are proportional to the slopes along the axis and the chord respectively. In this case, the data from the reference [17] is used and the natural frequencies obtained are compared with those given in the same paper.

In each case, as the system of partial differential equations is coupled and its closed form solution is difficult to obtained mathematically, the system of equations is solved by Finit Element Method. This comprises of discretizing the blade into a finite number of elements, approximating the deflections over each element by suitable shape functions, computing element stiffness and mass matrices thereby converting the system of the partial differential equations to a matrix eigen-value problem, assembling the element stiffness and mass matrices, applying the essential boundary conditions and solving the eigen-value problem. Finite elemen method, as described above, is employed because results obtained by this method converge to the exact solution with the refinement of the mesh of elements. Two noded beam elements and four noded plate elements have been employed in Chapters 2 and 3 respectively. To solve the eigen value problem, a NAG subroutine titled F02AEF [30] is made use of. This subroutine uses Householder's decomposition and QL algorithm to compute eigen-values and eigen vectors. The graphs of Chapter 2 have been plotted using GPGS graphic subroutine.

CHAPTER 2

VIBRATIONS OF BLADE AS A CANTILEVER BEAM

2.1 BLADE AS A BEAM:

When the length of the blade is large as compared to its other dimensions, it can be treated as a beam. This chapter deals with the problem of free vibration of the stationary turbine blade idealized as

a. untwisted straight beam of asymmetric aerofoil cross-section and,

b. untwisted as well as pre-twisted straight cantilever beams of rectangular cross-section.

The effects of stagger angle, taper, rotary inertia and shear deformation are neglected.

In the case of an asymmetric aerofoil-section, its centroid and the centre of flexure are distinct. This gives rise to coupled bending-bending-torsional vibration even when the pre-twist of the beam is zero. The turbine blading has asymmetric aerofoil section with one principal area moment of inertia much greater than the other.

For an untwisted uniform beam of rectangular cross-section, it is observed that the flapwise bending, the chordwise bending and the torsional modes of vibration are all uncoupled. But, in the case of a pre-twisted beam with rectangular cross-section, bending-bending coupled motion occurs

due to pre-twist and torsion is still uncoupled as the centroid and the flexural centre are coincident.

2.2 DERIVATION:

Consider a pre-twisted straight cantilever beam of an asymmetric cross-section as shown in the Figure 2.1. Let u, v and θ be chordwise displacement, flapwise displacement and angular displacement about the axis of torsion of the beam respectively. The strain energy [2] of this beam is given by the expression:

$$V = \frac{1}{2}\int_0^l \Big\{ E\Big[I_{yy}\Big(\frac{\partial^2 u}{\partial z^2}\Big)^2 + 2I_{xy}\Big(\frac{\partial^2 u}{\partial z^2}\Big)\Big(\frac{\partial^2 v}{\partial z^2}\Big) + I_{xx}\Big(\frac{\partial^2 v}{\partial z^2}\Big)^2\Big] + C\Big(\frac{\partial\theta}{\partial z}\Big)^2 - C_2\Big(\frac{\partial^2\theta}{\partial z^2}\Big)^2\Big\}\, dz \qquad (2.1.a)$$

where I_{yy}, I_{xx} and I_{xy} are the area moments and product of inertia of the cross-section of the beam about the reference axes. The term containing I_{xy} is because of the pre-twist γ and it causes coupling of flapwise and chordwise bending. Let I_{22} and I_{11} be the principal area moments of inertia of the cross-section. The area moments and product of inertia depend on the angle between the reference axes and the principal axes of the section and their transformation is given by

$$\underline{\underline{I}} = \overset{\cdots}{I}_{av}\,\underline{\underline{1}} + I_{mu}\,\underline{\underline{A}}_b \quad \text{(see reference [8])}$$

where

$$\underline{\underline{I}} = \begin{bmatrix} I_{yy} & I_{xy} \\ I_{xy} & I_{xx} \end{bmatrix}, \quad \underline{\underline{A}}_b = \begin{bmatrix} \cos\frac{2\pi z}{l} & \sin\frac{2\pi z}{l} \\ \sin\frac{2\pi z}{l} & -\cos\frac{2\pi z}{l} \end{bmatrix},$$

$$I_{av} = \frac{I_{22} + I_{11}}{2} \quad \text{and} \quad I_{mu} = \frac{I_{22} - I_{11}}{2} \qquad (2.1.b)$$

C is the torsional stiffness of the cross-section and is given by

$$C = C_1 + C_3\left(\frac{\pi}{l}\right)^2 \qquad (2.1.c)$$

The term containing C_2 in equation (2.1.a) is the contribution of fibre-bending during torsion.

C_1, C_2 and C_3 are the functions of material properties and geometry of the beam. The terms corresponding to these constants are due to the total torque on the cross-section that comprises of

i) St. Venant torsional moment: This is because of the twisting as well as warping of the cross-section,

ii) torque due to pre-twist: The pre-twist augments the warping of the cross-section thereby increasing the restoring torque and

iii) torque due to fibre-bending: The tendency of the beam to reduce warping thus trying to retain the planeness of the cross-section during the deformation results in the additional torque which is the consequence of the bending of each individual fibre.

The expression for the kinetic energy [2] of the beam is,

$$T = \frac{1}{2}\rho\int_0^1\Big\{A\Big[\Big(\frac{\partial u}{\partial t}\Big)^2 + \Big(\frac{\partial v}{\partial t}\Big)^2 + 2\Big(r_y\frac{\partial u}{\partial t} - r_x\frac{\partial v}{\partial t}\Big)\Big(\frac{\partial\theta}{\partial t}\Big)\Big] + I_{cf}\Big(\frac{\partial\theta}{\partial t}\Big)^2\Big\}dz \qquad (2.2.a)$$

where r_x and r_y are the co-ordinate distances between the centroid and the centre of torsion (which is assumed to be coincident with the flexural centre of the cross-section). The term containing r_x and r_y in the equation (2.2.a) is due to asymmetry of the cross-section which is responsible for the coupling of torsion and flapwise as well as chordwise bending. If the cross-section is symmetric, say rectangular, the centroid and flexural centre are not distinct and the torsional mode is decoupled from the bending modes. I_{cf} is the polar moment of inertia about the centre of flexure and is given by

$$I_{cf} = I_{cm} + A(r_x^2 + r_y^2) \qquad (2.2.b)$$

where I_{cm} is polar moment of inertia about the centroid of the cross-section.

Applying Hamilton's principle,

$$\delta\int_{t_1}^{t_2}(T - V)dt = 0\,, \qquad (2.3.a)$$

One obtains the governing equation of coupled bending-bending-torsion vibrations as

$$\left[\underline{\underline{A}}\ \underline{u}''\right]'' + \underline{\underline{B}}\ \underline{u}'' + \underline{\underline{C}}\ \ddot{\underline{u}} = \underline{0} \qquad (2.3.b)$$

in which dash (') and dot (.) represent partial derivatives with respect to spatial co-ordinate z and time t respectively, and

$$\underline{u}^T = [u\ v\ \theta], \quad \underline{\underline{A}} = \begin{bmatrix} EI_{yy} & EI_{xy} & 0 \\ EI_{xy} & EI_{xx} & 0 \\ 0 & 0 & -C_2 \end{bmatrix},$$

$$\underline{\underline{B}} = \text{diag}\,[0\ 0\ -C], \quad \underline{\underline{C}} = \begin{bmatrix} \varrho A & 0 & \varrho Ar_y \\ 0 & \varrho A & -\varrho Ar_x \\ \varrho Ar_y & -\varrho Ar_x & \varrho I_{cf} \end{bmatrix} \qquad (2.3.c)$$

It is obvious that tensor $\underline{\underline{A}}$ causes bending-bending coupling whereas $\underline{\underline{C}}$ causes bending-bending-torsion coupling.

At the fixed end, the deflections and the deflection derivatives are zero. Hence, the geometric boundary conditions are

$$\text{at} \quad z = 0, \quad \underline{u} = 0 \quad \text{and} \quad \underline{u}' = 0 \qquad (2.3.d)$$

At free end, the shear forces, the bending moments and the twisting moment are all zero. Hence, the natural boundary conditions are

$$\text{at} \quad z = l, \quad \underline{\underline{A}}\ \underline{u}'' = \underline{0}$$
$$\text{and} \quad \left[\underline{\underline{A}}\ \underline{u}''\right]' + \underline{\underline{B}}\ \underline{u}' = \underline{0} \qquad (2.3.e)$$

2.3 CASE 1:

First of all, consider an untwisted straight beam of asymmetric aerofoil cross-section in which case the effect of fibre bending is negligible i.e., for $\Gamma = 0$, C_2 is small and hence neglected and

$$\underline{\underline{A}} = \text{diag}\left[EI_{22} \quad EI_{11} \quad 0\right] \qquad (2.3.f)$$

The tensor $\underline{\underline{C}}$ remains unaltered resulting in bending-bending-torsional coupled mode of vibration.

As closed form solution of the system of equations (2.3.b), (2.3.d) and (2.3.e) is difficult to obtain, to solve it, one has to apply one of the approximate numerical methods such as Galerkin, Collocation, FDM, FEM, etc. Since the results obtained by FEM converge to the exact solution with the refinement of the mesh, FEM is utilized to solve this system of equations.

For this case, since C_2 is small, in the variational functional of the equation (2.3.a), the highest derivatives of u and v are of the second order and that of Θ of the first order. Hence, the principal derivatives are (i) $\frac{\partial u}{\partial z}$ and u, (ii) $\frac{\partial v}{\partial z}$ and v and (iii) Θ. The compatibility condition states that the approximating functions should be such that u, $\frac{\partial u}{\partial z}$, u, $\frac{\partial v}{\partial z}$, Θ should be continuous across the interelement boundary. The highest derivative occurring in the variation is of the order three for u and v and of the order for one Θ (as seen from the natural boundary conditions, equation (2.3.e)). Hence, the completeness condition implies that the shape

functions for u and v should be cubic polynomials and those for Θ should be linear polynomials.

The beam is discretized into a finite number of two noded elements. A typical element is shown in the Figure 2.2. There are five degrees of freedom at each node. Let u_1, $\frac{\partial u_1}{\partial z}$, v_1, $\frac{\partial v_1}{\partial z}$, Θ_1 be local degrees of freedom at one of the nodes of the element and u_2, $\frac{\partial u_2}{\partial z}$, v_2, $\frac{\partial v_2}{\partial z}$, Θ_2 be those at another node. One can then express $\underline{u}$ at any point P on the element as

$$\underline{u} = \underline{\underline{S}}\, \underline{U}^e\, e^{i\omega t} \qquad (2.4.a)$$

where

$$(\underline{U}^e)^T = \left[U_1 \quad \frac{\partial U_1}{\partial z} \quad V_1 \quad \frac{\partial V_1}{\partial z} \quad \Theta_1 \quad U_2 \quad \frac{\partial U_2}{\partial z} \quad V_2 \quad \frac{\partial V_2}{\partial z} \quad \Theta_2 \right]$$

and

$$\underline{\underline{S}} = \begin{bmatrix} P_1 & P_2 & 0 & 0 & 0 & P_3 & P_4 & 0 & 0 & 0 \\ 0 & 0 & P_1 & P_2 & 0 & 0 & 0 & P_3 & P_4 & 0 \\ 0 & 0 & 0 & 0 & Q_1 & 0 & 0 & 0 & 0 & Q_2 \end{bmatrix} \qquad (2.4.b)$$

Here P_i's ($i = 1$ to 4) and Q_j's ($j = 1$ and 2) are the functions of the local co-ordinate ξ.

For e^{th} element, the relationship between ξ and the global co-ordinate z is given by

$$\xi = \frac{1}{a}(z - z_c)$$

where

$$a = \frac{z_{e+1} - z_e}{2}$$

is the half-length of the element,

$$z_c = \frac{z_{e+1} + z_e}{2}$$

is the global co-ordinate of the mid-point and

z_e and z_{e+1} are the global co-ordinates of the nodes.

(2.5)

The expressions for P_i's and Q_j's which satisfy the convergence criteria are

$$P_1 = \frac{1}{4}(2 - 3\xi + \xi^3)$$

$$P_2 = \frac{a}{4}(1 - \xi - \xi^2 + \xi^3)$$

$$P_3 = \frac{1}{4}(2 + 3\xi - \xi^3)$$

$$P_4 = \frac{a}{4}(-1 - \xi + \xi^2 + \xi^3) \qquad (2.6)$$

$$Q_1 = \frac{1}{2}(1 - \xi)$$

$$Q_2 = \frac{1}{2}(1 + \xi)$$

Substituting $\underline{u} = \underline{\underline{S}}\ \underline{U}^e\ e^{i\omega t}$ as an approximate solution in the equation (2.3.b), one gets the residue

$$\underline{\varepsilon}^e = \{[\underline{\underline{A}}\ \underline{\underline{S}}"]" + \underline{\underline{B}}\ \underline{\underline{S}}"\}\ \underline{U}^e - \omega^2\ \underline{\underline{C}}\ \underline{\underline{S}}\ \underline{U}^e \qquad (2.7.a)$$

$\underline{\varepsilon}^e$ is a non-zero vector albeit it tends to zero as the size of the element is reduced.

Applying Galerkin's method, one gets

$$\int_{z_e}^{z_{e+1}} \underline{\underline{S}}^T \underline{\varepsilon}^e \, dz = \underline{0} \qquad (2.7.b)$$

whence the system of partial differential equations simplifies to the following Eigen-value problem

$$\underline{\underline{K}}^e \underline{U}^e - \lambda \underline{\underline{M}}^e \underline{U}^e = \underline{R}^e \qquad (2.7.c)$$

where $\lambda = \omega^2$ and the expressions for the element stiffness matrix, the element mass matrix and the element stress-resultant vector are as follows:

$$\underline{\underline{K}}^e = \int_{z_e}^{z_{e+1}} \left[(\underline{\underline{S}}^T)'' (\underline{\underline{A}})(\underline{\underline{S}})'' - (\underline{\underline{S}}^T)' (\underline{\underline{B}})(\underline{\underline{S}})' \right] dz \qquad (2.7.d)$$

$$\underline{\underline{M}}^e = \int_{z_e}^{z_{e+1}} (\underline{\underline{S}}^T)(\underline{\underline{C}})(\underline{\underline{S}}) dz \qquad (2.7.e)$$

and

$$\underline{R}^e = \left[- \underline{\underline{S}}^T (\underline{\underline{A}} \, \underline{u}'')' + \underline{\underline{B}} \, \underline{u}' + (\underline{\underline{S}}^T)' (\underline{\underline{A}} \, \underline{u}'') \right]_{z_e}^{z_{e+1}} \qquad (2.7.f)$$

To evaluate the element stiffness and mass matrices, one changes the variable from the global co-ordinate z to the local co-ordinate ξ given by the equation (2.5). Then

$$dz = a \, d\xi \,, \quad \frac{\partial}{\partial z} = \frac{1}{a} \frac{\partial}{\partial \xi} \quad \text{and} \quad \frac{\partial^2}{\partial z^2} = \frac{1}{a^2} \frac{\partial^2}{\partial \xi^2} \qquad (2.7.g)$$

and the limits of the integration change from z_e and z_{e+1} to -1 and 1 respectively, thus

$$\int_{z_e}^{z_{e+1}} f(z)dz = a \int_{-1}^{1} f(z_c + a\xi)d\xi \qquad (2.7.h)$$

After integration, one obtains element stiffness matrix and element mass matrix given by the equations (2.7.i) and (2.7.j) respectively. These are symmetric positive definite matrices of the order 10 x 10. The element matrices, thus obtained, are assembled together to obtain the global stiffness matrix and the global mass matrix according to the standard procedure of FEM and each of them is singular.

To solve this system of equations, one partitions the global matrices after applying the geometric boundary conditions

$$\text{at} \quad z = 0, \quad U_1 = 0, \frac{\partial U_1}{\partial z} = 0, \quad V_1 = 0, \frac{\partial V_1}{\partial z} = 0, \quad \Theta_1 = 0 \qquad (2.7.k)$$

and hence one gets an eigen-value problem as

$$\underline{\underline{K}}\,\underline{U} - \lambda\,\underline{\underline{M}}\,\underline{U} = \underline{0} \qquad (2.7.l)$$

Solution of this equation gives the eigen-values λ_i's in number equal to the order of $\underline{\underline{K}}$ or $\underline{\underline{M}}$ and the corresponding eigen-vectors.

$$
[K]^e = \begin{bmatrix}
\frac{3EI_{22}}{2a^3} & \frac{3EI_{22}}{2a^2} & 0 & 0 & 0 & -\frac{3EI_{22}}{2a^3} & \frac{3EI_{22}}{2a^2} & 0 & 0 & 0 \\
\frac{3EI_{22}}{2a^2} & \frac{2EI_{22}}{a} & 0 & 0 & 0 & -\frac{3EI_{22}}{2a^3} & \frac{EI_{22}}{a} & 0 & 0 & 0 \\
0 & 0 & \frac{3EI_{11}}{2a^3} & \frac{3EI_{11}}{2a^2} & 0 & 0 & 0 & -\frac{3EI_{11}}{2a^3} & \frac{3EI_{11}}{2a^2} & 0 \\
0 & 0 & \frac{3EI_{11}}{2a^2} & \frac{2EI_{11}}{a} & 0 & 0 & 0 & -\frac{3EI_{11}}{2a^2} & \frac{EI_{11}}{a} & 0 \\
0 & 0 & 0 & 0 & \frac{C}{2a} & 0 & 0 & 0 & 0 & -\frac{C}{2a} \\
-\frac{3EI_{22}}{2a^3} & -\frac{3EI_{22}}{2a^2} & 0 & 0 & 0 & \frac{3EI_{22}}{2a^3} & -\frac{3EI_{22}}{2a^2} & 0 & 0 & 0 \\
\frac{3EI_{22}}{2a^2} & \frac{EI_{22}}{a} & 0 & 0 & 0 & -\frac{3EI_{22}}{2a^2} & \frac{2EI_{22}}{a} & 0 & 0 & 0 \\
0 & 0 & -\frac{3EI_{11}}{2a^3} & -\frac{3EI_{11}}{2a^2} & 0 & 0 & 0 & \frac{3EI_{11}}{2a^3} & -\frac{3EI_{11}}{2a^2} & 0 \\
0 & 0 & \frac{3EI_{11}}{2a^2} & \frac{EI_{11}}{a} & 0 & 0 & 0 & -\frac{3EI_{11}}{2a^2} & \frac{2EI_{11}}{a} & 0 \\
0 & 0 & 0 & 0 & -\frac{C}{2a} & 0 & 0 & 0 & 0 & \frac{C}{2a}
\end{bmatrix} \qquad (2.7.1)
$$

$$[M]^e = \rho \begin{bmatrix}
\frac{26Aa}{35} & \frac{22Aa^2}{105} & 0 & 0 & -\frac{7Aar_x}{10} & \frac{9Aa}{35} & -\frac{13Aa^2}{105} & 0 & 0 & -\frac{3Aar_x}{10} \\
\frac{22Aa^2}{105} & \frac{8Aa^3}{105} & 0 & 0 & -\frac{Aa^2r_x}{5} & \frac{13Aa^2}{105} & -\frac{2Aa^3}{35} & 0 & 0 & -\frac{2Aa^2r_x}{15} \\
0 & 0 & \frac{26Aa}{35} & \frac{22Aa^2}{105} & \frac{7Aar_y}{10} & 0 & 0 & \frac{9Aa}{35} & -\frac{13Aa^2}{105} & \frac{3Aar_y}{10} \\
0 & 0 & \frac{22Aa^2}{105} & \frac{8Aa^3}{105} & \frac{Aa^2r_y}{5} & 0 & 0 & \frac{13Aa^2}{105} & -\frac{2Aa^3}{35} & \frac{2Aa^2r_y}{15} \\
-\frac{7Aar_x}{10} & -\frac{Aa^2r_x}{5} & \frac{7Aar_y}{10} & \frac{Aa^2r_y}{5} & \frac{2aI_{cf}}{3} & -\frac{3Aar_x}{10} & \frac{2Aa^2r_x}{15} & \frac{2Aa^2r_y}{15} & -\frac{2Aa^2r_y}{15} & \frac{aI_{cf}}{3} \\
\frac{9Aa}{35} & \frac{13Aa^2}{105} & 0 & 0 & -\frac{3Aar_x}{10} & \frac{26Aa}{35} & -\frac{22Aa^2}{105} & 0 & 0 & -\frac{7Aar_x}{10} \\
-\frac{13Aa^2}{105} & -\frac{2Aa^3}{35} & 0 & 0 & \frac{2Aa^2r_x}{15} & -\frac{22Aa^2}{105} & \frac{8Aa^3}{105} & 0 & 0 & \frac{Aa^2r_x}{5} \\
0 & 0 & \frac{9Aa}{35} & \frac{13Aa^2}{105} & \frac{3Aar_y}{10} & 0 & 0 & \frac{26Aa}{35} & -\frac{22Aa^2}{105} & \frac{7Aar_y}{10} \\
0 & 0 & -\frac{13Aa^2}{105} & -\frac{2Aa^3}{35} & -\frac{2Aa^2r_y}{15} & 0 & 0 & -\frac{22Aa^2}{105} & \frac{8Aa^3}{105} & -\frac{Aa^2r_y}{5} \\
-\frac{3Aar_x}{10} & -\frac{2Aa^2r_x}{10} & \frac{3Aar_y}{10} & \frac{2Aa^2r_y}{15} & \frac{aI_{cf}}{3} & -\frac{7Aar_x}{10} & \frac{Aa^2r_x}{5} & \frac{7Aar_y}{10} & -\frac{Aa^2r_y}{5} & \frac{2aI_{cf}}{3}
\end{bmatrix} \qquad (2.7.j)$$

2.3.1 SOLUTION:

To solve the equation (2.7.1) for the eigen-values and eigen-vectors, the NAG subroutine F02AEF [30] has been utilized. According to this, for the system of equations $[A]\{x\} = \lambda[B]\{x\}$, where [A] must be a symmetric square matrix and [B] must be a positive definite symmetric square matrix, all the eigen-values and eigen-vectors are computed using Householder's decomposition and QL algorithm. Note that the eigen-values λ_i represent the square of the natural frequencies ω_i of vibration of the beam. As the continuous system is approximated by a set of finite number of elements, the infinite number of degrees of freedom corresponding to the continuous system is reduced to a finite number, thereby making the approximated model stiffer than the actual system. Obviously, with the increase in the number of elements, the number of degrees of freedom increases, the overall stiffness of the approximated model decreases and consequently the eigen-values converge to their lower bounds.

During the computation of the results, it was experienced that as the number of elements was increased, the first eigen-value oscillated about a mean value whereas the higher order eigen-values converged. It was conjectured that this could possibly be due to

(i) $I_{yy} >> I_{xx}$, leading to the ill-conditioning of the system of equations; and

(ii) the number of iterations in the NAG subroutine are

fixed but unknown and the user cannot exercise any control over it. The eigen-values are the roots of the polynomial given by

$$|A - \lambda B| = 0 \qquad (2.7.m)$$

The higher roots of the polynomial equation (2.7.m) can be obtained by neglecting the lower degree terms while for finding out the lower eigen-values, in particular the lowest one, one has to consider all the terms. Consequently, higher roots can be computed with fewer number of iteratilns whereas the first few roots can be obtained only after a considerable number of iterations. Therefore, it is quite apt that the value of the first eigen-value is not a converged value within the number of iterations fixed by the subroutine itself.

Since the number of iterations is beyond the control of the user, to mitigate the problem of oscillating first natural frequency, one solves the system as an inverse eigen-value problem so that the lowest mode becomes the highest mode of the new system. Thus, in lieu of solving the system of equations (2.7.1), one solves

$$\underline{\underline{M}}\,\underline{U} - \mu\,\underline{\underline{K}}\,\underline{U} = \underline{0} \qquad (2.7.n)$$

where $\mu_i = \dfrac{1}{\lambda_{(n-i+1)}}$

The number of eigen-values $_i$ for the new system of equations

is equal to the order of $\underline{\underline{K}}$ or $\underline{\underline{M}}$. The eigen-values are the inverse of the square of i^{th} natural frequency ω_i. Hence, the first (lowest) eigen-value λ_1 of the actual system becomes the last (highest) eigen-value μ_n of the inverse system ($\mu_n = \frac{1}{\lambda_1}$). The converged value of λ_1 is the reciprocal of the converged value of μ_n. It is verified that this indeed yields converged eigen-values with the increase in the number of elements. The number of frequencies and the corresponding eigen-vectors obtained is equal to the order of the partitioned stiffness or mass matrix and can be found out by subtracting the number of the specified degrees of freedom from the total number of degrees of freedom of the approximated model.

2.3.2 DATA AND RESULTS:

The results have been obtained for the blade used in [12] so that the results can be compared with it. The data for the aerofoil section are:

Geometric properties

$I_{11} = 3.49634 \times 10^{-11}$ m^4

$I_{22} = 2.79291 \times 10^{-9}$ m^4

$l = 0.1524$ m

$r_x = 1.9304 \times 10^{-4}$ m

$r_y = 1.1938 \times 10^{-3}$ m

$A = 5.8967 \times 10^{-5}$ m^2

$E = 213.7388$ GPa

$C = 9.1485978$ N/m

$\rho = 7858.3702$ kg/m^3

Material properties

To test whether the given cross-section can be treated as a beam or not, the Zukovsky transformation 22 was made use of. The Zukovsky transformation, which maps an aero-foil-section in -plane to a circle in z-plane as shown in the Figure 2.3, is given by

$$\zeta = z + \frac{a^2}{z}, \quad \text{where} \quad \zeta = \xi + i\eta \quad \text{and} \quad z = x + iy \tag{2.8.a}$$

Refer to Appendix I for details.

The transformation gives the chord length b and the maximum thickness h as

$$b = 4(I_{22}/A)^{1/2} \tag{2.8.b}$$

and

$$h = 3(2I_{11}/A)^{1/2} \tag{2.8.c}$$

From equations (2.8.b) and (2.8.c) one gets

$$\frac{1}{b} = \frac{1}{4}(A/I_{22})^{1/2} = 5.53606$$

and

$$\frac{b}{h} = \frac{4}{3}(I_{22}/2I_{11})^{1/2} = 8.426461$$

As the length is large in comparison with the chord length and the maximum thickness, for the data considered, the blade can be treated as a beam.

Results: For the data given above, the computed results upto fifth mode are given in the Table 2.1 and are compared with those obtained in the reference [12] by (a) analytical method and (b) Ritz-Galerkin method. The physical identification of the frequencies was done by drawing the corresponding mode shapes (they are not shown here). The results were obtained for fourteen elements of equal length.

Table 2.1

Comparison of results for $\frac{l}{b} = 5.53606$, $\frac{b}{h} = 8.426461$

Method	Description of modes	Frequency in Hz				
		First bending in YY I	Second bending in YY II	First bending in XX III	First torsion IV	Third bending in YY V
Analytical results [12]		96.9	606.5	841.2	1072.9	1699.0
Results by Ritz-Galerkin method [12]		96.5	604.9	842.0	1089.4	1694.9
Present results		96.8	606.3	843.3	1078.5	1697.8

2.4 CASE 2:

Having studied the vibrations of untwisted cantilever beam of aerofoil cross-section, we now focus our attention on the pre-twisted cantilever beams of rectangular cross-section. For a rectangular section, the centroid and the flexural centre are coincident. So, the torsional mode is uncoupled; but the flapwise bending and chordwise bending are coupled because of the pre-twist. If the pre-twist is zero, both the bending modes also get decoupled. In this case, it is assumed that the effect of fibre-bending is not negligible.

If b and h are the breadth and the height of the beam of rectangular cross-section, the expressions for the constants C_1, C_2 and C_3 in equations (2.1.a) and (2.1.c) are given as follows:

(i)

$$C_1 = \frac{1}{3} Gbh^3 \{1 - \frac{192}{\pi^5} \frac{h}{b} \sum_{n=1,3,5\ldots} \frac{1}{n^5} \tanh \frac{n\pi}{2} \frac{b}{h}\} \qquad (2.9.a)$$

where C_1 is the St. Venant torsional stiffness [19].

(ii)

$$C_3 = \frac{Ehb^5}{180} \qquad (2.9.b)$$

where C_3 is the torsional stiffness due to pre-twist [10].

(iii)

$$C_2 = \frac{Eb^3h^3}{144} \qquad (2.9.c)$$

where C_2 is the constant for the fibre-bending [20].

In this case, the tensors $\underline{\underline{A}}$ and $\underline{\underline{C}}$ of the equation (2.3.b) are given by

$$\underline{\underline{A}} = \underline{\underline{A}}_1 + EI_{mu}\,\underline{\underline{A}}_2 \quad \text{and} \quad \underline{\underline{C}} = \text{diag}\,[\rho A,\ \rho A,\ \rho I_{cf}] \qquad (2.10.a)$$

where

$$\underline{\underline{A}}_1 = \text{diag}[EI_{av},\ EI_{av},\ -C_2]$$

and (2.10.b)

$$\underline{\underline{A}}_2 = \begin{bmatrix} \cos\frac{2\pi z}{l} & \sin\frac{2\pi z}{l} & 0 \\ \sin\frac{2\pi z}{l} & -\cos\frac{2\pi z}{l} & 0 \\ 0 & 0 & 0 \end{bmatrix}$$

As the fibre-bending is considered, the maximum derivative of Θ in the functional is of second order. Hence the principal derivatives for Θ are $\frac{\partial\Theta}{\partial z}$ and Θ. The convergence criteria states that Θ should also be expressed by Hermitian polynomials. P_i's. Hence, in equation (2.4.a), one gets

$$(\underline{U}^e)^T = \lfloor\, U_1\ \frac{\partial U_1}{\partial z}\ V_1\ \frac{\partial V_1}{\partial z}\ \Theta_1\ \frac{\partial\Theta_1}{\partial z}\ U_2\ \frac{\partial U_2}{\partial z}\ V_2\ \frac{\partial V_2}{\partial z}\ \Theta_2\ \frac{\partial\Theta_2}{\partial z}\,\rfloor \qquad (2.11.a)$$

and

$$\underline{\underline{S}} = \begin{bmatrix} P_1 & P_2 & 0 & 0 & 0 & 0 & P_3 & P_4 & 0 & 0 & 0 & 0 \\ 0 & 0 & P_1 & P_2 & 0 & 0 & 0 & 0 & P_3 & P_4 & 0 & 0 \\ 0 & 0 & 0 & 0 & P_1 & P_2 & 0 & 0 & 0 & 0 & P_3 & P_4 \end{bmatrix} \qquad (2.11.b)$$

The expressions for element stiffness matrix and mass matrix are the same as those in the previous case. With the incorporation of fibre-bending, the order of the element stiffness and mass matrices becomes 12 x 12 and can be evaluated by simplifying integrations are discussed in the Section 2.3.

Applying the geometric boundary conditions,

$$\text{at } z = 0,\ U_1 = 0,\ \frac{\partial U_1}{\partial z} = 0,\ V_1 = 0,\ \frac{\partial V_1}{\partial z} = 0,\ \Theta_1 = 0,\ \frac{\partial \Theta_1}{\partial z} = 0 \qquad (2.11.c)$$

which physically mean that the deflection and the deflection derivatives are zero at the fixed end of the cantilever beam, one obtains the eigen-value problem on the lines similar to the Section 2.3.

2.4.1 DATA AND RESULTS:

The results have been obtained for the blades used in [18], [8] and [17] so that the results can be compared with these cases.

2.4.1.a Blade 1: The effect of the fibre-bending:

Data: $b = 0.0254$ m

$h = 0.001727$ m — Geometric properties

$l = 0.1524$ m

$\gamma = \frac{\pi}{4}$ rad

$E = 206.85$ GPa

$G = 82.74$ GPa Material properties

$\rho = 7858.3702$ kg/m^3

As $\frac{l}{b} = 6$ and $\frac{b}{h} = 14.706$, the length is larger than the other dimensions and hence the blade can be treated as a beam.

Results: For this data, the frequencies obtained are given in the Table 2.2 and their modes are identified as discussed in the previous case. The beam was discretized into 14 elements.

Table 2.2

Frequencies for $\frac{l}{b} = 6$, $\frac{b}{h} = 14.706$ and $\gamma = \frac{\pi}{4}$ rad

Mode No.	Frequency in Hz					
	Bending in Y-Y direction (coupled)		Bending in X-X direction (coupled)		Torsion (uncoupled)	
	Present results	Results of ref. [18]	Present results	Results of ref. [18]	Present results	Results of ref. [18]
1	62.027	62.17	977.620	977.62	756.421	758.15
2	310.005	310.18	5930.315	5926.49	2298.804	2349.61
3	1232.751	1232.54	-	-	3928.691	4162.77
4	2223.903	2223.51	-	-	5702.135	6242.28

It is observed that the frequencies of bending-bending modes tally with the results given in the reference [18], but the torsional frequencies do not agree with the results. This

is because in the reference [18],

(i) the section has been approximated to the elliptic form and the corresponding formula for the St. Venant torsional stiffness has been used and

(ii) the contribution of the pre-twist to the torsional stiffness is neglected and also it is assumed that the fibre-bending effect is negligible.

2.4.1.b Blade 2: The effect of the pre-twist:

Let us now study the effect of pre-twist on the vibrations of the beam with rectangular cross-section. For this, the data used in the reference [8] is considered. Using this data, the frequencies are found out for different values of pre-twist. The graph of reference [8] is shown in Figure 2.4.a.

Data: $b = 0.0254$ m

$h = 0.00635$ m Geometric properties

$l = 0.3048$ m

$E = 206.85$ GPa

$G = 82.74$ GPa Material properties

$\rho = 7858.7302$ kg/m^3

For this data, $\frac{l}{b} = 12$ and $\frac{b}{h} = 4$ and hence the blade is treated as a beam. The frequencies for various values of pre-twist are tabulated with their modes identified and their trend with respect to the pre-twist in the Table 2.3. The beam is discretised into fifteen elements.

Table 2.3

The effect of pre-twist on the frequencies for $\frac{l}{b} = 12$, $\frac{b}{h} = 4$

Pre-twist in rad \ Mode	Frequency in Hz								
	I	II	III	IV	V	VI	VII	VIII	IX
	Y-Y bending	X-X bending	Y-Y bending	Y-Y bending	torsion (uncoupled)	X-X bending	Y-Y bending	X-Y bending	torsion (uncoupled)
0	56.648	226.593	355.055	995.042	1216.913	1439.983	1955.093	3249.381	3665.574
$\pi/6$	56.886	211.642	381.694	949.546	1217.324	1491.793	1949.248	3258.255	3666.803
$\pi/4$	57.029	198.425	408.780	905.318	1217.574	1562.767	1926.250	3243.700	3667.551
$\pi/3$	57.351	185.029	440.716	859.238	1217.842	1638.410	1903.460	3225.509	3668.350
$\pi/2$	58.182	161.088	551.026	776.180	1218.440	1696.503	1942.339	3186.277	3670.137
Trend	↑	↓	↑	↓	↑	↑	↓	↓	↑

N.B.: ↑ – increasing; ↓ – decreasing.

It is observed that each mode has got a specific trend of variation with respect to the angle-of-pre-twist. The first frequency corresponding to the first Y-Y bending mode increases with pre-twist. The second mode corresponding to the first X-X bending mode decreases with pre-twist and the fifth mode corresponding to the first torsional mode increases with the pre-twist. This is because the beam becomes stiffer for the Y-Y bending and the torsion whereas it becomes more flexible for the X-X bending at their first modes. The graphs in the Figure 2.4 depict the trends of the first nine frequencies with respect to the angle of pre-twist. These trends tally with those illustrated graphically in the reference [8], Figure 2.4.a.

2.4.1.c Blade 3: The effect of the pre-twist and the dimensions:

For this blade, the data from the reference [17] is utilized.

Data: $h = 0.025$ m Thickness

$E = 200.00$ GPa

$\mu = 0.3$ (Poisson's ratio) Material properties

$\rho = 7800$ kg/m^3

For this data and for four different geometries, the non-dimensionalized frequencies given by

$$\omega_o = \omega l^2 \sqrt{\rho h/D} \qquad (2.12)$$

where $$D = \frac{Eh^3}{12(1 - \mu^2)}$$

are computed for the different angles of pre-twist and are tabulated in the Tables 2.4, 2.5, 2.6 and 2.7. The beams are discretised into seven elements.

Table 2.4

$\frac{l}{b} = 1, \quad \frac{b}{h} = 5$

Pre-twist γ rad	Non-dimensionalized frequency ω_o							
	I	II	III	IV	V	VI	VII	VIII
	Y-Y bending	Torsion	X-X bending	Torsion	Y-Y bending	Torsion	Torsion	Y-Y bending
0	3.354	5.940	16.771	18.739	21.044	34.040	49.225	59.311
π/12	3.363	6.154	16.087	18.615	21.989	31.534	45.221	58.487
π/6	3.371	6.410	14.743	19.389	24.006	32.846	47.103	56.908
π/4	3.379	6.677	13.432	20.196	26.440	34.213	49.062	54.722
π/3	3.397	6.954	12.257	21.034	29.086	35.633	51.099	52.315
π/2	3.448	7.539	10.363	22.804	34.383	38.632	55.399	48.041

Table 2.5

$\frac{l}{b} = 1, \quad \frac{b}{h} = 20$

Pre-twist γ rad	Non-dimensionalized frequency ω_o							
	I	II	III	IV	V	VI	VII	VIII
	Y-Y bending	Torsion	Torsion	Y-Y bending	Torsion	Torsion	Y-Y bending	X-X bending
0	3.354	5.364	19.693	21.030	34.889	52.348	59.067	67.082
$\pi/12$	3.466	9.453	128.592	20.560	48.436	69.459	58.375	70.140
$\pi/6$	3.464	11.949	36.142	19.079	61.226	87.800	57.282	77.227
$\pi/4$	3.395	14.167	42.850	17.211	72.590	104.097	56.123	86.339
$\pi/3$	3.417	16.229	49.090	15.462	83.160	119.255	54.638	96.053
$\pi/2$	3.474	20.105	50.811	12.567	103.016	147.730	50.695	109.752

Table 2.6

$\frac{l}{b} = 3, \quad \frac{b}{h} = 5$

Pre-twist γ rad	Non-dimensionalised frequency ω_o							
	I	II	III	IV	V	VI	VII	VIII
	Y-Y bending	X-X bending	Torsion	Y-Y bending	Torsion	Y-Y bending	Torsion	X-X bending
0	3.354	16.771	17.780	21.030	55.101	59.067	97.622	105.150
$\pi/12$	3.363	16.057	17.808	21.989	53.365	58.487	91.250	106.081
$\pi/6$	3.371	14.743	17.898	24.006	54.138	56.908	91.712	108.357
$\pi/4$	3.379	13.430	17.996	26.440	54.432	54.722	92.210	110.079
$\pi/3$	3.397	12.257	18.100	29.086	54.748	52.315	92.746	109.734
$\pi/2$	3.449	10.363	18.333	34.383	55.453	48.041	93.939	106.366

Table 2.7

$\frac{l}{b} = 3, \quad \frac{b}{h} = 20$

Pre-twist γ rad	Non-dimensionalised frequency ω_o							
	I	II	III	IV	V	VI	VII	VIII
	Tor-sion	Y-Y ben-ding	Tor-sion	Tor-sion	Tor-sion	Tor-sion	Y-Y ben-ding	Y-Y ben-ding
0	1.903	3.354	5.908	10.466	15.695	20.138	21.030	59.067
$\pi/12$	7.269	3.456	21.986	37.246	53.412	70.821	20.560	58.375
$\pi/6$	10.308	3.463	31.179	52.819	75.744	100.433	19.079	57.282
$\pi/4$	12.813	3.398	38.756	65.654	94.151	124.840	17.211	56.124
$\pi/3$	15.062	3.420	45.560	77.180	110.680	145.756	15.462	54.638
$\pi/2$	19.175	3.467	57.999	98.253	140.898	186.824	12.566	50.595

The trends of the frequencies versus the pre-twist for the four different aspects ratios are plotted in the graphs — Figures 2.5, 2.6, 2.7 and 2.8 — corresponding to the Tables 2.4, 2.5, 2.6 and 2.7 respectively. As surmised, some modes either exhibit the trends contradictory to those in the reference [17] or do not exhibit a definite trend, for the short blade is treated as a beam here.

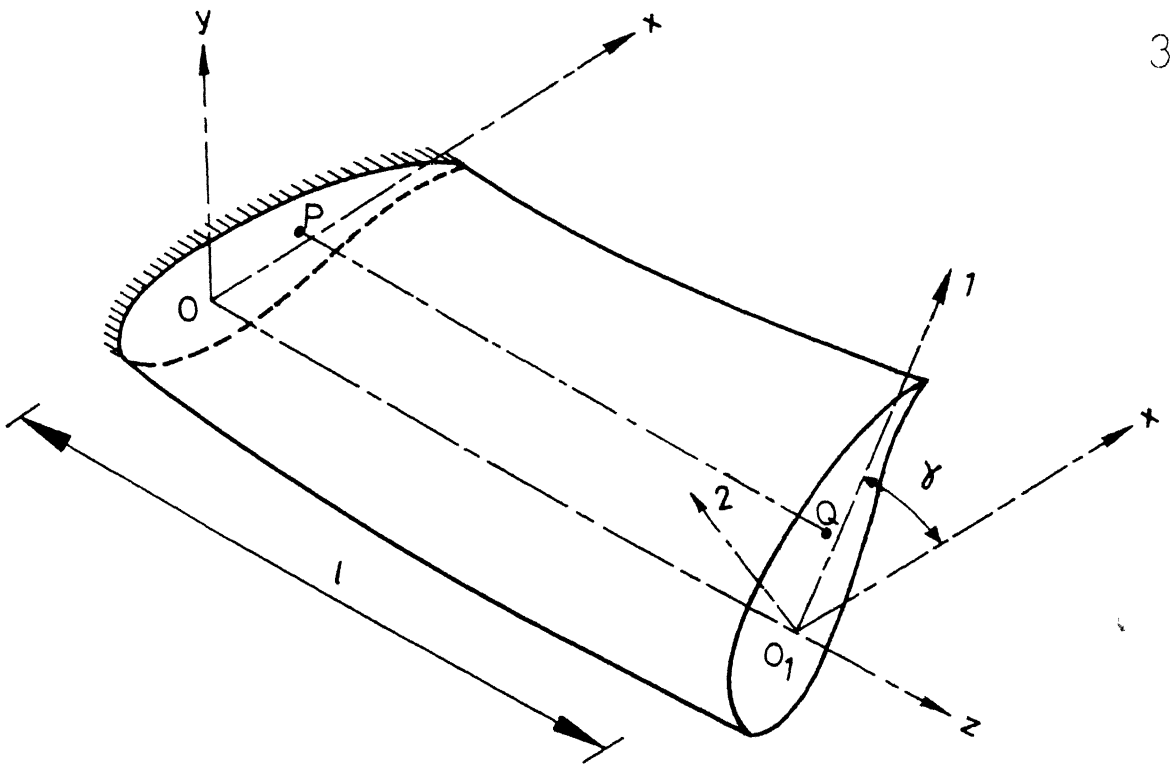

x,y,z, ≡ Reference axes; 1, 2 ≡ principal axes

OO_1 ≡ Flexural axis ; PQ ≡ Centroidal axis

γ ≡ Total angle of pretwist.

FIG.2.1.a PRE-TWISTED CANTILEVER BEAM

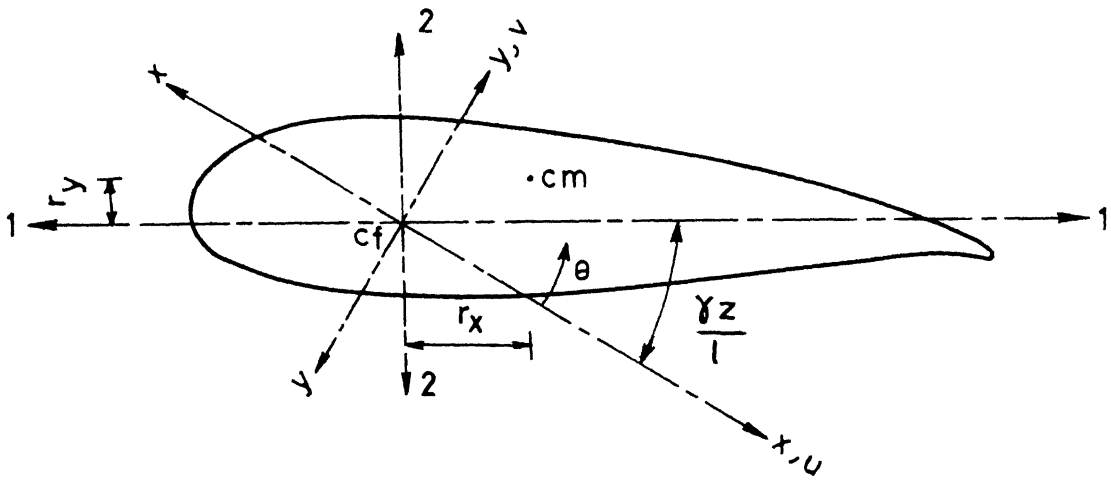

cf ≡ centre of flexure; cm ≡ centre of mass.

FIG.2.1.b CROSS-SECTION OF THE BEAM

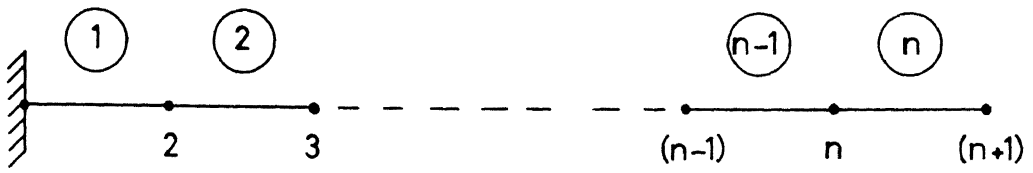

N.B. The encircled numbers represent the element numbers.

FIG.2.2a DISCRETIZATION OF THE CANTILEVER BEAM INTO A FINITE NUMBER OF TWO-NODED ELEMENTS.

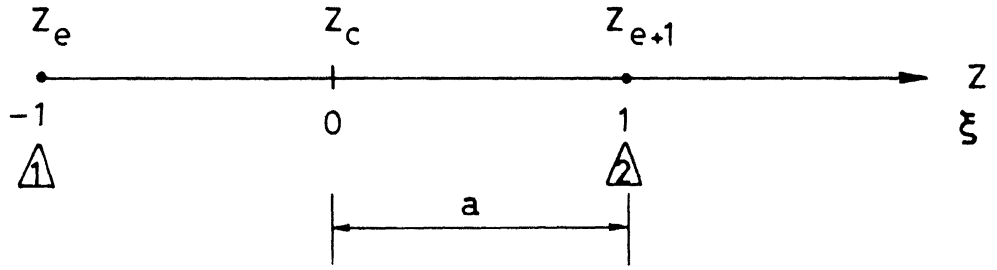

e^{th} element

Z - Global co-ordinate, ξ - Local co-ordinate

a - Half the length of the element

Numbers inscribed in the triangle represent local node numbers.

FIG. 2.2.b A TYPICAL TWO-NODED ELEMENT

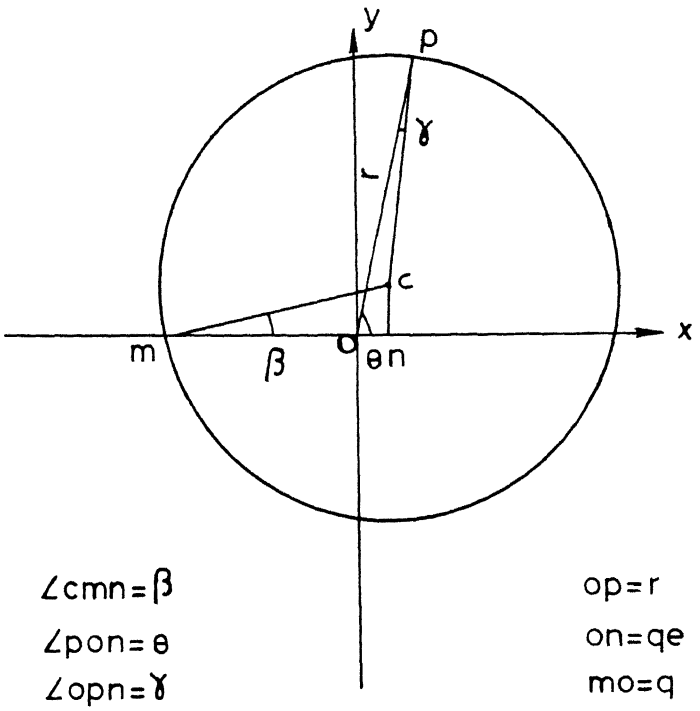

$\angle cmn = \beta$

$\angle pon = \theta$

$\angle opn = \gamma$

$op = r$

$on = qe$

$mo = q$

$cn = s$

$cp = t$

Transformation $\zeta = z + \frac{q^2}{z}$

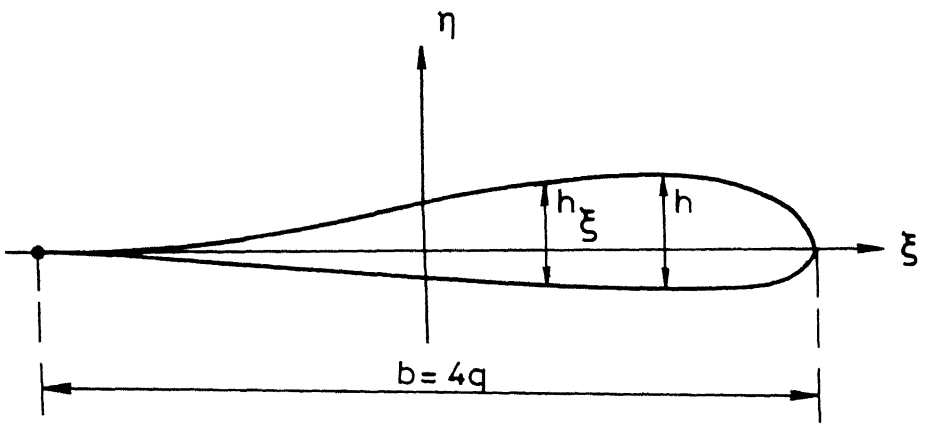

FIG. 2.3 ZUKOVSKY TRANSFORMTION

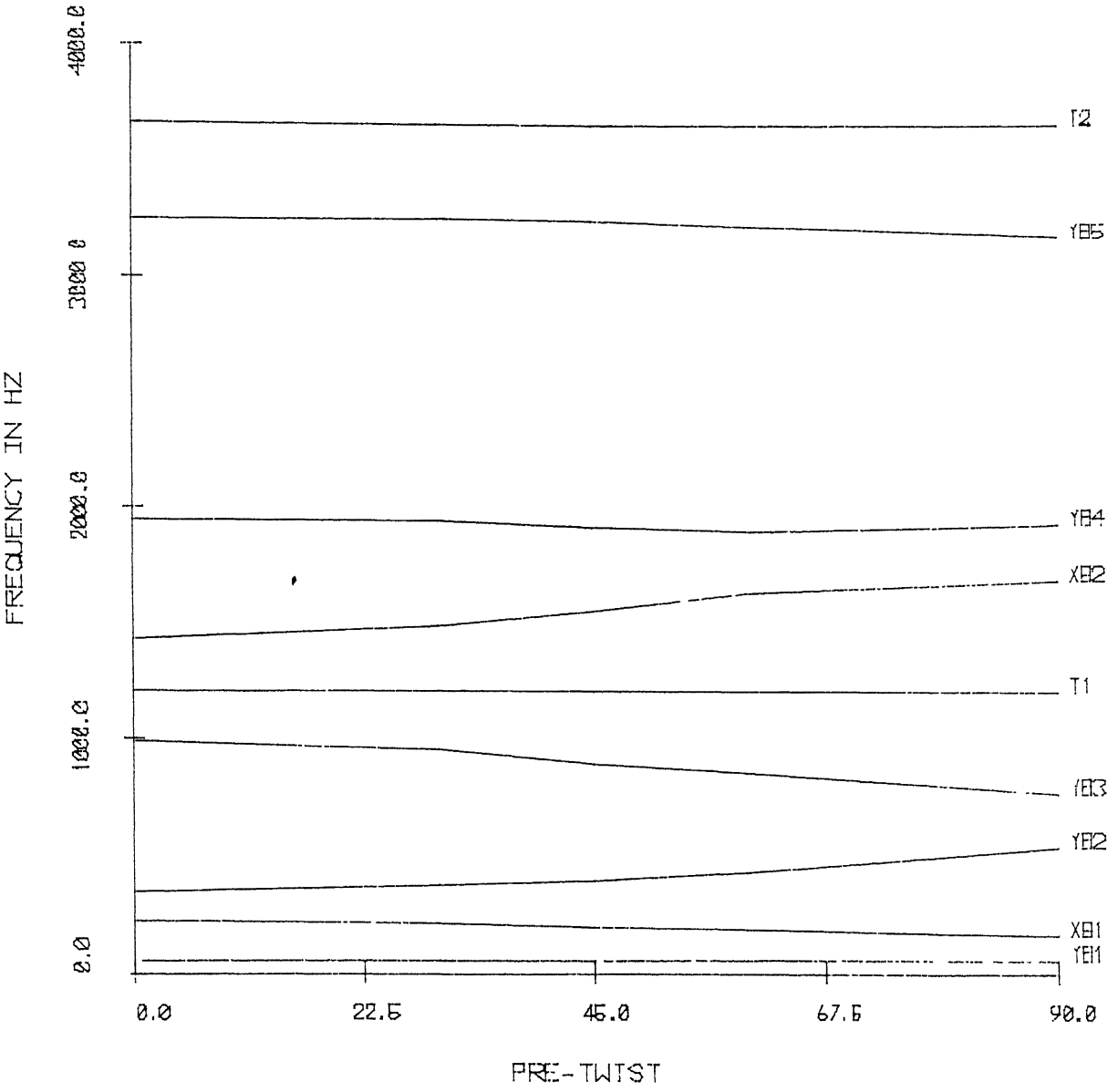

FIG. 2.4 GRAPH OF
FREQUENCY VERSUS PRE-TWIST
FOR L/B=12 AND B/H=4

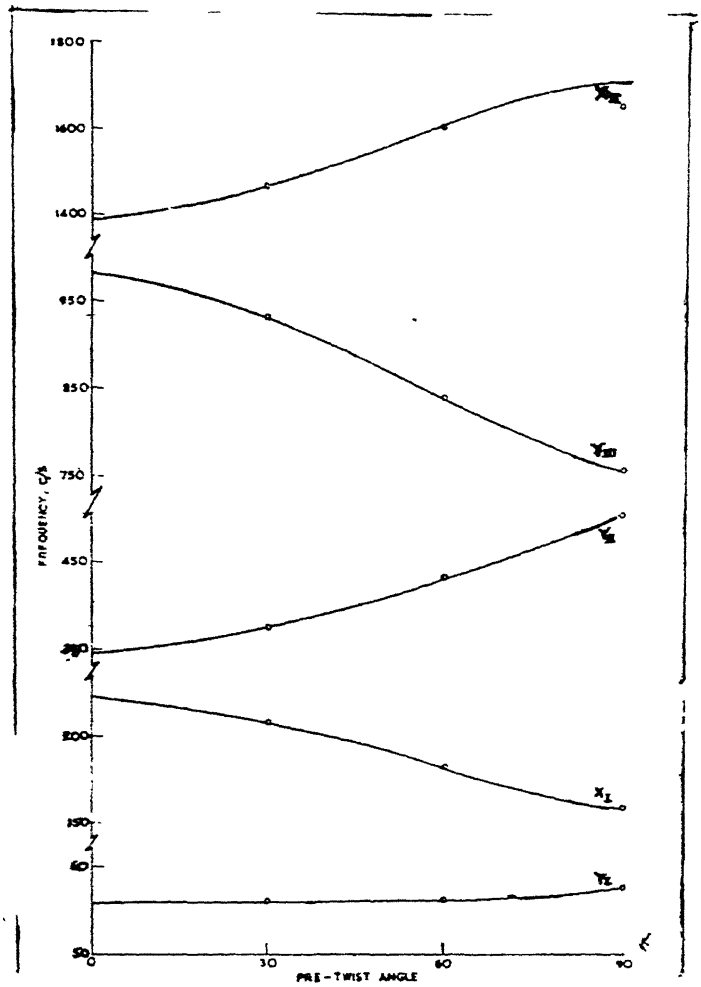

FIG. 2.4.a GRAPH OF
FREQUENCY VERSUS PRE-TWIST
FOR L/B = 12 AND B/H = 4
REFERENCE 8

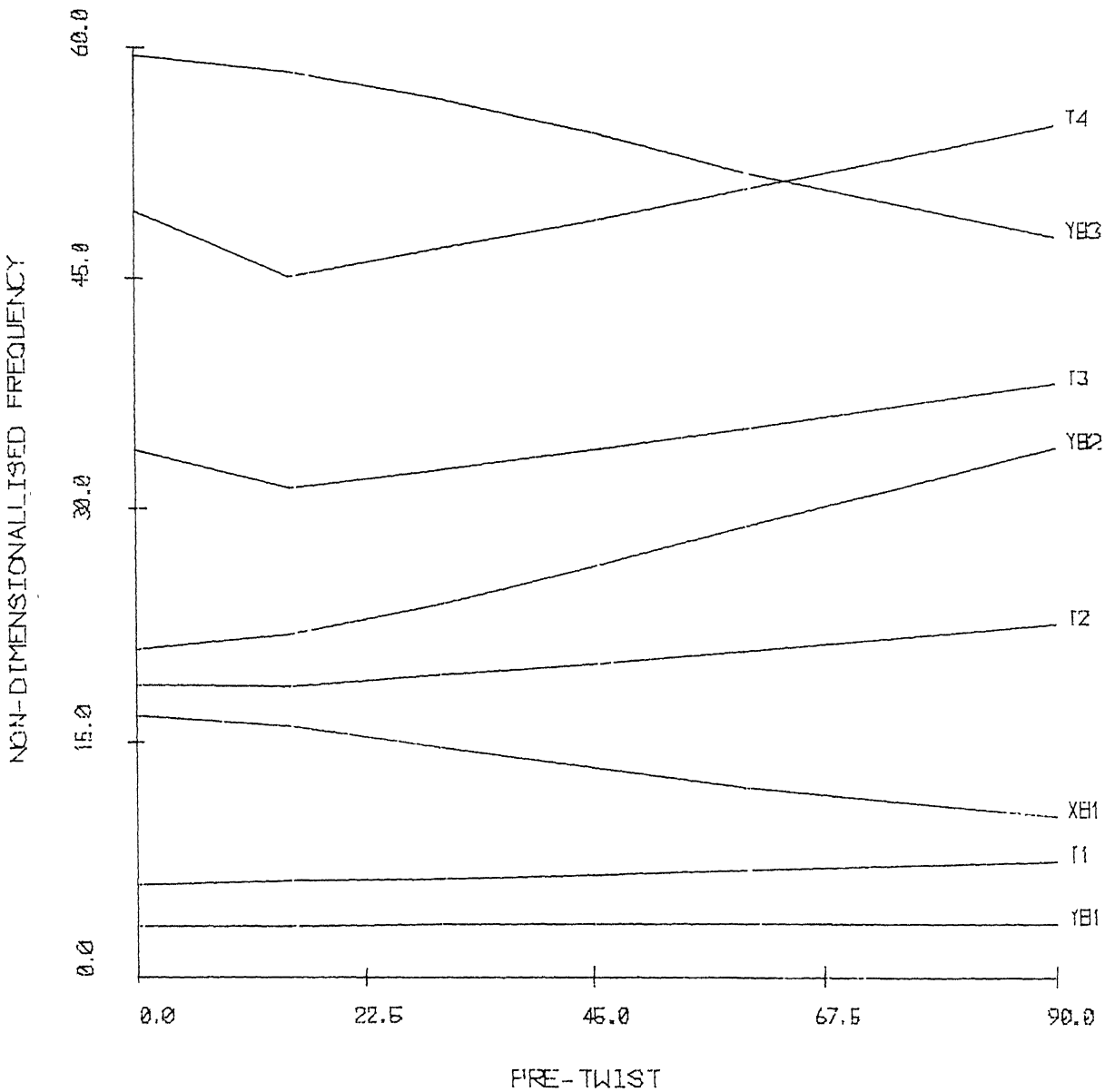

FIG.2.5 GRAPH OF
FREQUENCY VERSUS PRE-TWIST
FOR L/B=1 AND B/H=5

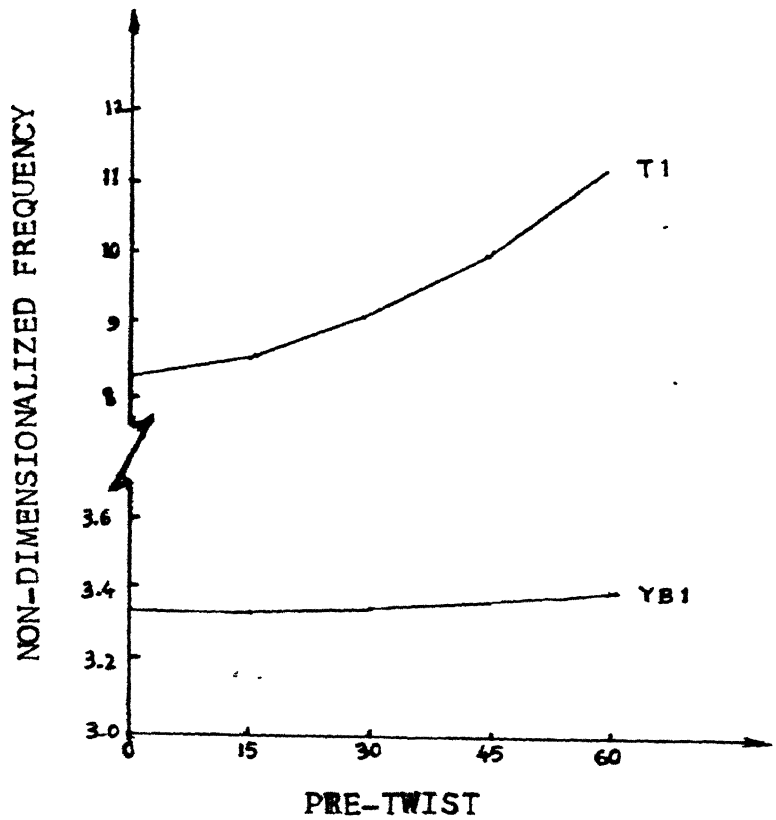

FIG. 2.5a GRAPH OF

FREQUENCY VERSUS PRE-TWIST

FOR L/B = 1 AND B/H = 5

REFERENCE 17

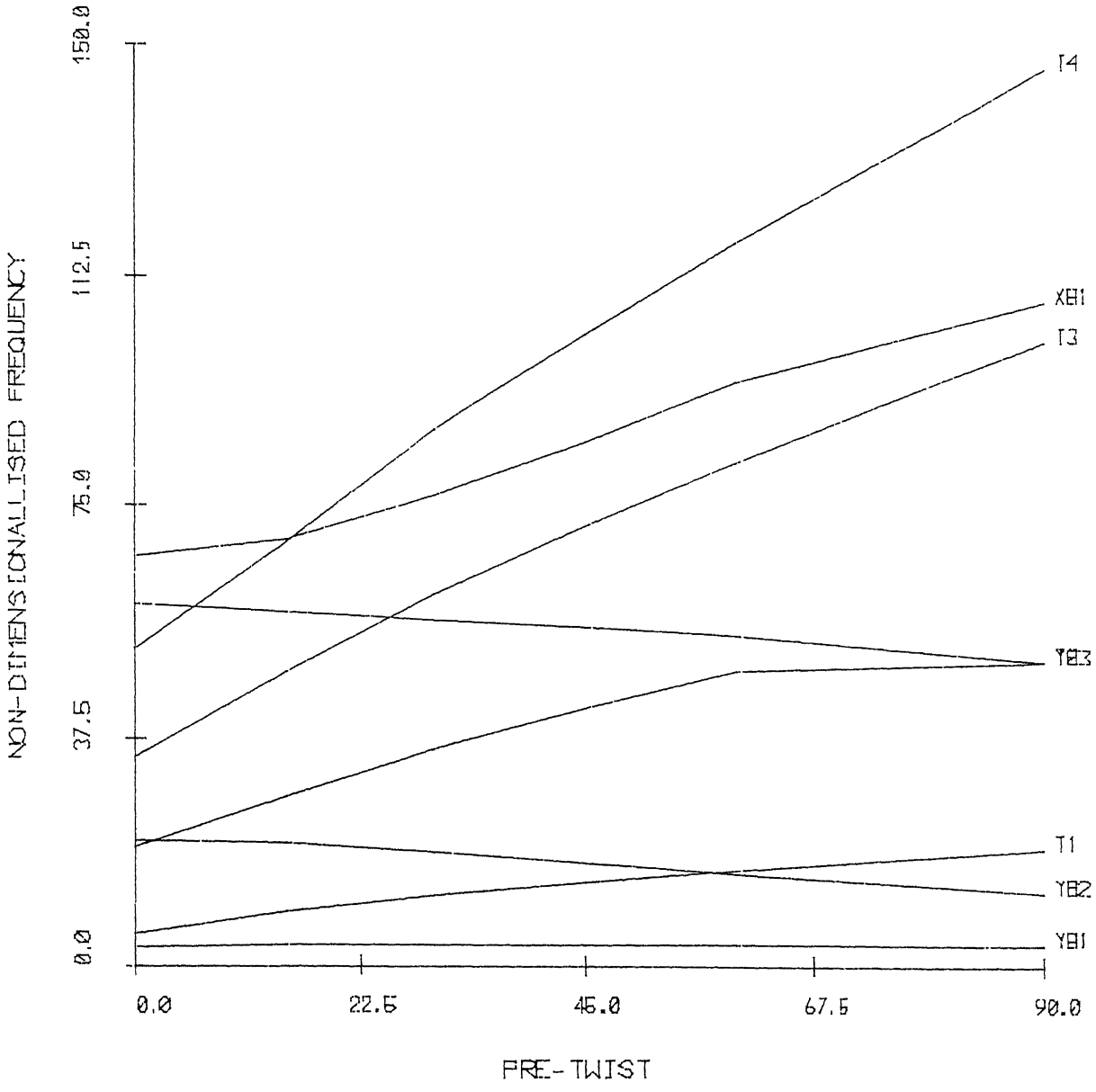

FIG.2.6 GRAPH OF
FREQUENCY VERSUS PRE-TWIST
FOR L/B=1 AND B/H=20

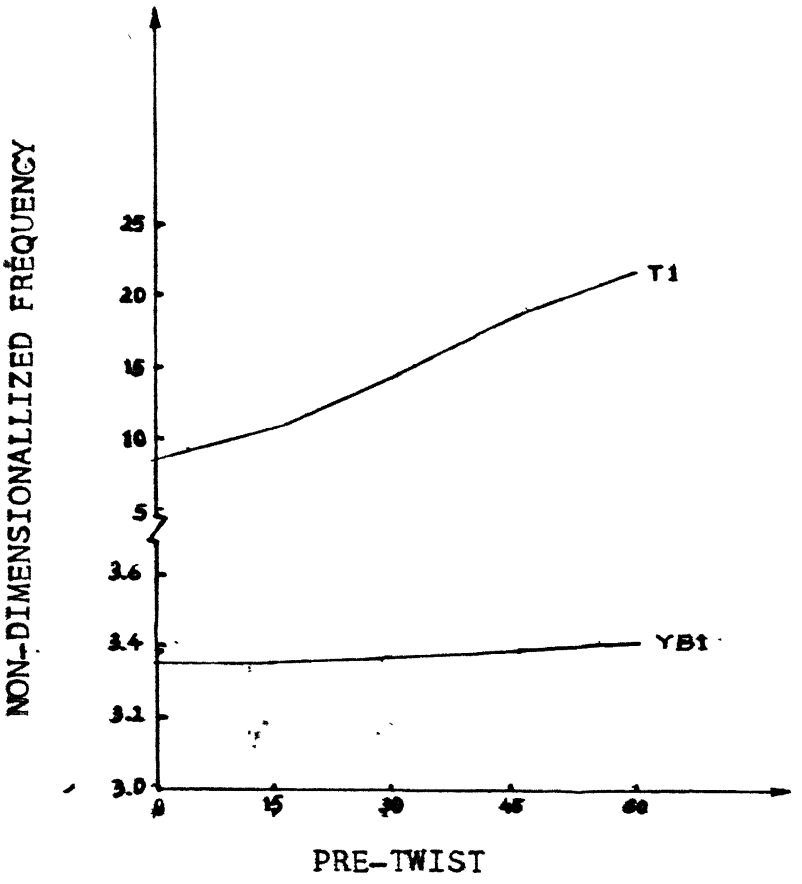

FIG. 2.6a GRAPH OF
FREQUENCY VERSUS PRE-TWIST
FOR L/B = 1 AND B/H = 20
REFERENCE 17

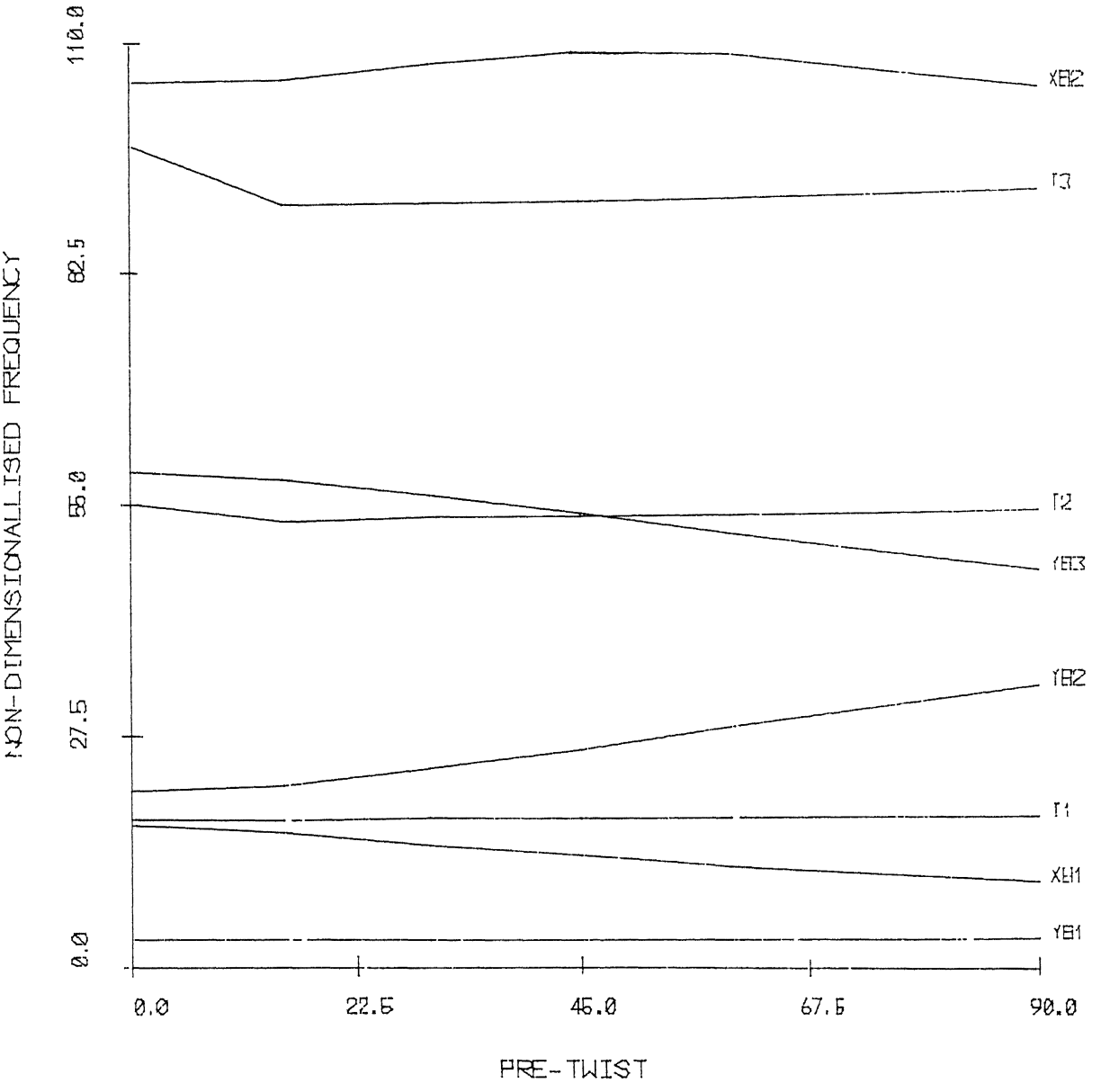

FIG.2.7 GRAPH OF
FREQUENCY VERSUS PRE-TWIST
FOR L/B=3 AND B/H=5

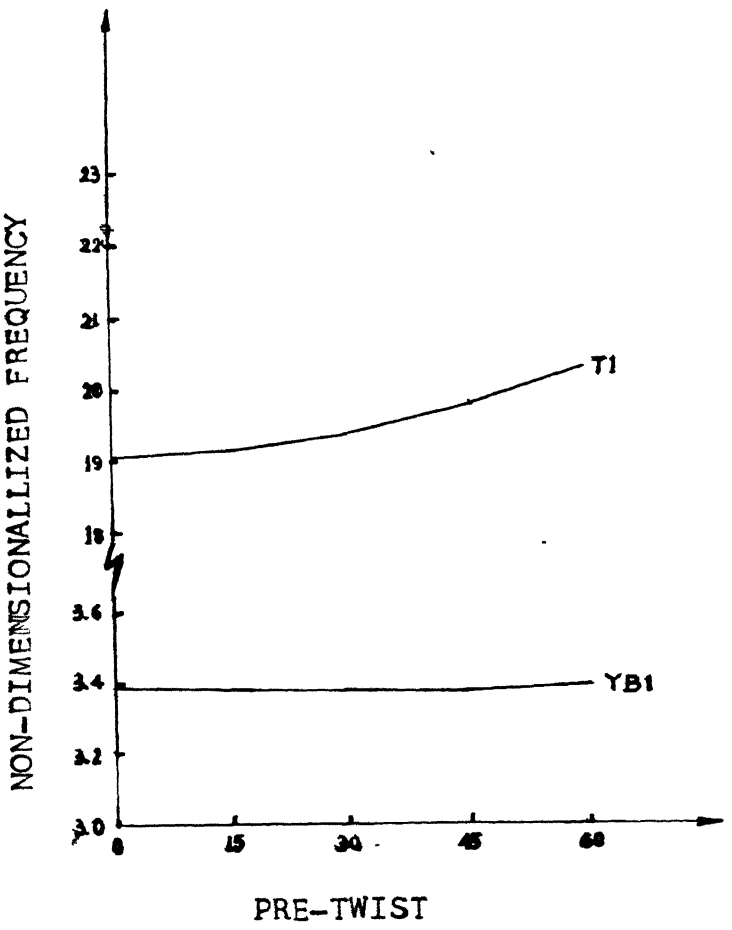

FIG. 2.7a GRAPH OF FREQUENCY VERSUS PRE-TWIST FOR L/B = 3 AND B/H = 5 REFERENCE 17

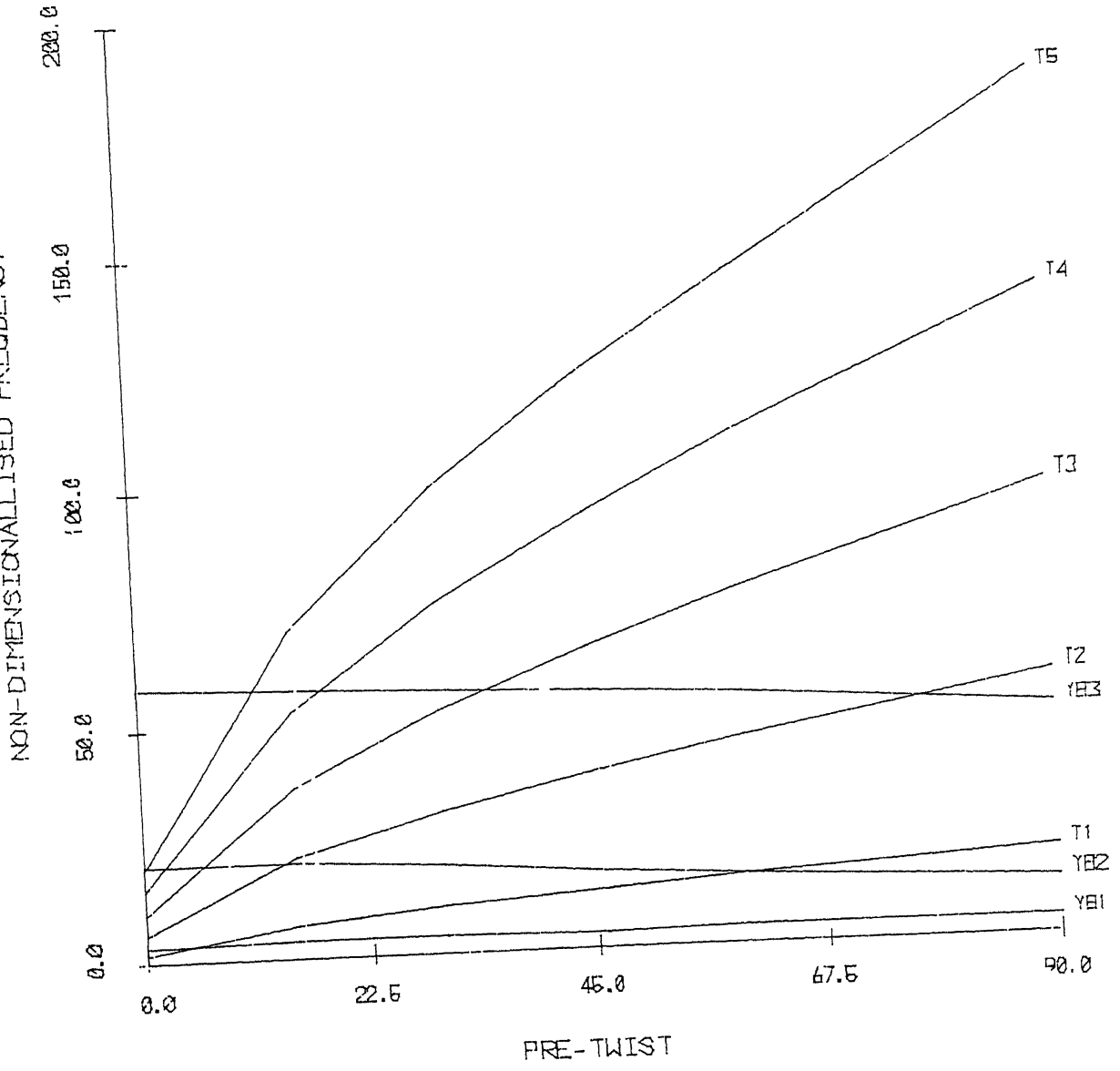

FIG.2.8 GRAPH OF
NON-DIMENSIONALLISED FREQUENCY VERSUS PRE-TWIST
FOR L/B=3 AND B/H=20

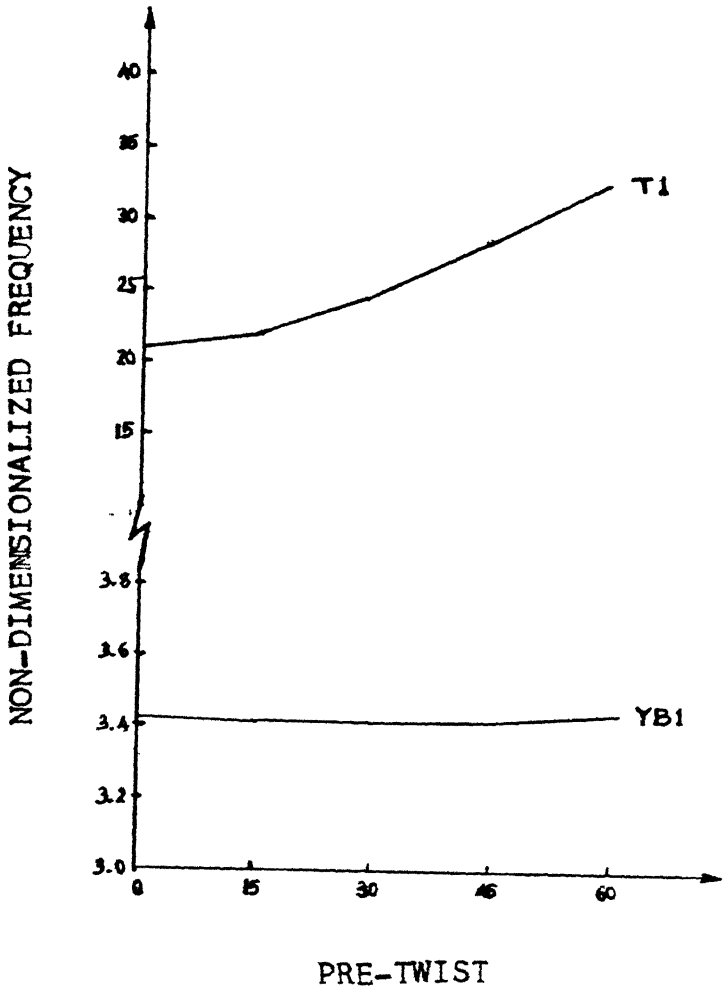

FIG. 2.8a GRAPH OF
FREQUENCY VERSUS PRE-TWIST
FOR L/B = 3 AND B/H = 20
REFERENCE 17

CHAPTER 3

VIBRATIONS OF BLADE AS A CANTILEVER PLATE

3.1 BLADE AS A PLATE:

When the length of the blade is short and is comparable to its cross-sectional dimensions, it tends to behave like a plate rather than a beam. If the blades are pre-twisted, they have geometric curvatures and torsion and hence behave like shells. When their pre-twist is zero, their geometric curvatures and torsion are zero and can be treated as a plate. A plate is defined as an object bounded by two flat surfaces. If the distance between these surfaces is very small as compared to the other dimensions of plate, it is called a thin plate, else it is said to be a thick plate. For the plates, where the thickness is very small as compared to either the overall dimension or to the wavelength corresponding to the highest frequency of interest, the effects due to shear deformation and rotary inertia can be neglected without affecting the accuracy of the solution [18].

This chapter deals with the study of free vibrations of a short blade treated as a uniform thin cantilever plate of rectangular cross-section, using FEM and neglecting rotary inertia and shear deformation.

3.2 DERIVATION:

For the thin plate shown in Figure 3.1, let w(x, y) be the displacement of a point on the middle surface along

z-axis. If we assume that the normal to the middle surface continues to be normal to it even after the deformation, then the displacements u and v of any arbitrary point (x, y, z) are given by

$$\underline{u} = z\nabla w \quad \text{i.e.} \quad u = z\frac{\partial w}{\partial x}$$

$$v = z\frac{\partial w}{\partial y} \qquad (3.1.a)$$

The most significant strain and stress components are

$$\underline{\underline{\epsilon}} = z\nabla\nabla w \quad \text{i.e.} \quad \epsilon_{xx} = z\frac{\partial^2 w}{\partial x^2}$$

$$\epsilon_{yy} = z\frac{\partial^2 w}{\partial y^2} \qquad (3.1.b)$$

$$\epsilon_{xy} = z\frac{\partial^2 w}{\partial x\,\partial y}$$

and

$$\underline{\underline{\sigma}} = \frac{E}{1-\mu^2}\left[\mu z\nabla^2 w\,\underline{\underline{1}} + (1-\mu)\,\underline{\underline{z}}\,\nabla\nabla w\right]$$

i.e.

$$\sigma_{xx} = \frac{Ez}{1-\mu^2}\left(\frac{\partial^2 w}{\partial x^2} + \mu\frac{\partial^2 w}{\partial y^2}\right)$$

$$\sigma_{yy} = \frac{Ez}{1-\mu^2}\left(\frac{\partial^2 w}{\partial y^2} + \mu\frac{\partial^2 w}{\partial x^2}\right) \qquad (3.1.c)$$

$$\sigma_{xy} = \frac{Ez}{1-\mu^2}\frac{\partial^2 w}{\partial x\,\partial y}$$

The stress-resultant over the thickness are defined by the relations

$$M_x = \int_{-h/2}^{h/2} \sigma_{xx}\, z\, dz$$

$$M_y = \int_{-h/2}^{h/2} \sigma_{yy}\, z\, dz$$

$$M_{xy} = \int_{-h/2}^{h/2} \sigma_{xy}\, z\, dz \qquad (3.2.a)$$

$$Q_x = \int_{-h/2}^{h/2} \sigma_{xz}\, dz$$

$$Q_y = \int_{-h/2}^{h/2} \sigma_{yz}\, dz$$

The stress-resultant M_x represents the bending moment per unit length on x-face about y-axis. Similarly M_y also represents the bending moment per unit length but on y-face about x-face. The quantity M_{xy} denotes the twisting moment per unit length about x-axis on x-face (or about y-axis on y-faces). The shear forces per unit length along z-axis on x and y-faces are represented by Q_x and Q_y. The relation between the moment tensor

$$\underline{\underline{M}}_m = \begin{bmatrix} M_x & M_{xy} \\ M_{xy} & M_y \end{bmatrix}$$

and the shear force vector

$$\underline{Q} = \begin{Bmatrix} Q_x \\ Q_y \end{Bmatrix}$$

is given by

$$\underline{Q} = \nabla \cdot \underline{\underline{M}}_m$$

The expressions for $\underline{\underline{M}}_m$ and $\underline{Q}$ in terms of w are:

$$\underline{\underline{M}}_m = D\left[\mu \nabla^2 w \, \underline{\underline{1}} + (1 - \mu) \nabla\nabla w\right] \qquad (3.2.b)$$

and

$$\underline{Q} = D \nabla (\nabla^2 w) \qquad (3.2.c)$$

where

$$D = \frac{Eh^3}{12(1 - \mu^2)} \qquad (3.2.d)$$

D is called the flexural rigidity of the plate.

The strain energy [16] of the plate is given by

$$V = \frac{D}{2} \int_A \left\{ (1 - \mu)(\nabla\nabla w) \cdot (\nabla\nabla w) + \mu (\nabla^2 w)^2 \right\} dA$$

$$= \frac{D}{2} \iint \left[\left(\frac{\partial^2 w}{\partial x^2}\right)^2 + \left(\frac{\partial^2 w}{\partial y^2}\right)^2 + 2\mu \left(\frac{\partial^2 w}{\partial x^2}\right)\left(\frac{\partial^2 w}{\partial y^2}\right) + 2(1 - \mu)\left(\frac{\partial^2 w}{\partial x \partial y}\right)^2 \right] dx \, dy \qquad (3.3)$$

The expression for the kinetic energy [26] of the plate is given as

$$T = \frac{1}{2} \rho h \iint \left(\frac{\partial w}{\partial t}\right)^2 dx \, dy \qquad (3.4)$$

Applying Hamilton's principle,

$$\delta \int_{t_1}^{t_2} (T - V) \, dt = 0 \qquad (3.5.a)$$

one obtains the governing equation of motion of the plate as

$$D \nabla^4 w + \rho h \frac{\partial^2 w}{\partial t^2} = 0 \qquad (3.5.b)$$

At the fixed end of the cantilever plate, the displacement and the displacement gradient are zero. Hence, the geometric boundary conditions at $x = 0$ are

i) $w = 0$ and $\frac{\partial w}{\partial x} = 0$

called the essential boundary conditions and (3.5.c)

ii) $\frac{\partial w}{\partial y} = 0$ and $\frac{\partial^2 w}{\partial x \partial y} = 0$

called the implied boundary conditions.

At the free boundary, the bending moment, the twisting moment and the shear force, are all zero. That is, $\underline{\underline{M}}_m \cdot \hat{n} = \underline{0}$ and $\underline{Q} \cdot \hat{n} = 0$, where $\hat{n}$ is the unit outward normal to the boundary. Hence, the natural boundary conditions for a rectangular plate shown in Figure 3.1 are

i) At $x = l$,

$$\frac{\partial^2 w}{\partial x^2} + \mu \frac{\partial^2 w}{\partial y^2} = 0$$

$$\frac{\partial^2 w}{\partial x \partial y} = 0$$

$$\frac{\partial^3 w}{\partial x^3} + \frac{\partial^3 w}{\partial x \partial y^2} = 0$$

ii) At $y = \pm \frac{b}{2}$,

$$\frac{\partial^2 w}{\partial y^2} + \mu \frac{\partial^2 w}{\partial x^2} = 0$$

$$\frac{\partial^2 w}{\partial x \partial y} = 0$$

$$\frac{\partial^3 w}{\partial x^2 \partial y} + \frac{\partial^3 w}{\partial y^3} = 0$$

(3.5.d)

At the governing equation is of the fourth order, two boundary conditions are needed at each boundary, whereas, in equation (3.5.d) three boundary conditions are obtained at each free boundary. In order to make the boundary conditions compatible, the boundary conditions for the shear force and the twisting moment are clubbed together [16] and hence, the equivalent natural boundary conditions at the free edges of the rectangular plate are

i) At $x = l$,

$$\frac{\partial^2 w}{\partial x^2} + \mu \frac{\partial^2 w}{\partial y^2} = 0$$

$$\frac{\partial^3 w}{\partial x^3} + (2 - \mu) \frac{\partial^3 w}{\partial x \partial y^2} = 0$$

ii) At $y = \pm \frac{b}{2}$,

$$\frac{\partial^2 w}{\partial y^2} + \mu \frac{\partial^2 w}{\partial x^2} = 0$$

$$\frac{\partial^3 w}{\partial y^3} + (2 - \mu) \frac{\partial^3 w}{\partial y \partial x^2} = 0$$

(3.5.e)

3.3 FINITE ELEMENT FORMULATION:

The closed form solution for a rectangular plate can be obtained explicitly if and only if the edges of the plate are simply supported. However, in the case of cantilever plate, closed form solution is difficult to obtain. Therefore, to study the vibrations of a cantilever plate, one has to make use of some numerical technique for the given plate(s) and here, the FEM has been opted for.

Consider the expression for the strain energy in equation (3.3). The highest derivatives of w in the expression of the strain energy are $\frac{\partial^2 w}{\partial x^2}$, $\frac{\partial^2 w}{\partial y^2}$ and $\frac{\partial^2 w}{\partial x \partial y}$. Therefore, the principal derivatives are w, $\frac{\partial w}{\partial x}$ and $\frac{\partial w}{\partial y}$. The compatibility condition states that these principal derivatives should be continuous across the inter-element boundaries. The highest derivative of w in boundary condition is of third order. Completeness condition states that the shape functions should be such that, as the element size reduces, the function and its derivatives upto the highest order accuracy in the variation of the strain energy are of finite values. This leads to the conclusion that the shape functions should be the product of at least cubic polynomials in ξ and η.

It is noted that a mesh of rectangular elements is used to suit the convenience of the geometry and because of the ease of finding the compatible shape functions. Consider a four noded rectangular plate element as shown in Figure 3.2. If (x_c, y_c) is the global mid-point of the element, p and q

are half the length and breadth of the element respectively, then a point within the element represented by the global co-ordinates (x, y) can be expressed in terms of the local co-ordinates as

$$\begin{Bmatrix} x \\ y \end{Bmatrix} = \begin{Bmatrix} x_c \\ y_c \end{Bmatrix} + \begin{bmatrix} p & 0 \\ 0 & q \end{bmatrix} \begin{Bmatrix} \xi \\ \eta \end{Bmatrix} \qquad (3.6)$$

where $-1 \leq \xi \leq 1$

and $-1 \leq \eta \leq 1$

The displacement of any point within the element in terms of the nodal degrees of freedom and the shape functions is

$$w = \underline{S} \cdot \underline{W}^e \, e^{i\omega t} \qquad (3.7)$$

where $\underline{W}^e$, the nodal displacement vector, is given by

$$(\underline{W}^e)^T = \left[w_1 \frac{\partial w_1}{\partial x} \frac{\partial w_1}{\partial y} \frac{\partial^2 w_1}{\partial x \partial y} w_2 \frac{\partial w_2}{\partial x} \frac{\partial w_2}{\partial y} \frac{\partial^2 w_2}{\partial x \partial y} \right.$$
$$\left. w_3 \frac{\partial w_3}{\partial x} \frac{\partial w_3}{\partial y} \frac{\partial^2 w_3}{\partial x \partial y} w_4 \frac{\partial w_4}{\partial x} \frac{\partial w_4}{\partial y} \frac{\partial^2 w_4}{\partial x \partial y} \right] \qquad (3.8.a)$$

Thus, there are sixteen degrees of freedom per element. The shape function vector is,

$$\underline{S} = \left[\phi_1 \phi_2 \phi_3 \phi_4 \phi_5 \phi_6 \phi_7 \phi_8 \phi_9 \phi_{10} \phi_{11} \phi_{12} \phi_{13} \phi_{14} \phi_{15} \phi_{16} \right] \qquad (3.8.b)$$

The expressions for ϕ_i's which satisfy the convergence criteria are:

For i = 1, 2, 3, 4,

$$\phi_{4i-3} = \frac{1}{16}(2 + 3\xi_i\xi - \xi_i\xi^3)(2 + 3\eta_i\eta - \eta_i\eta^3)$$

$$\phi_{4i-2} = \frac{p}{16}(-\xi_i - \xi + \xi_i\xi^2 + \xi^3)(2 + 3\eta_i\eta - \eta_i\eta^3)$$

$$\phi_{4i-1} = \frac{q}{16}(2 + 3\xi_i\xi - \xi_i\xi^3)(-\eta_i - \eta + \eta_i\eta^2 + \eta^3)$$

$$\phi_{4i} = \frac{pq}{16}(-\xi_i - \xi + \xi_i\xi^2 + \xi^3)(-\eta_i - \eta + \eta_i\eta^2 + \eta^3) \qquad (3.9)$$

Substituting $w = \underline{S} \cdot \underline{W}^e e^{i\omega t}$ in equation (3.5), one gets the residue ε^e

$$\varepsilon^e = D(\nabla^4 \underline{S}) \cdot \underline{W}^e - \rho h \omega^2 \underline{S} \cdot \underline{W}^e$$

which can be rewritten as

$$\varepsilon^e = D\left\{\left[\frac{\partial^4 \underline{S}}{\partial x^4} + 2\mu\frac{\partial^4 \underline{S}}{\partial x^2 \partial y^2} + \frac{\partial^4 \underline{S}}{\partial y^2}\right] \cdot \underline{W}^e + 2(1-\mu)\left(\frac{\partial^4 \underline{S}}{\partial x^2 \partial y^2}\right) \cdot \underline{W}^e\right\}$$

$$- \rho h \omega^2 \underline{S} \cdot \underline{W}^e \qquad (3.10.a)$$

Applying Galerkin's method,

$$\int_{x_e}^{x_{e+1}} \int_{y_e}^{y_{e+1}} \underline{S}\, \varepsilon^e \, dx\, dy = \underline{0}$$

$$\therefore \left(\int_{x_e}^{x_{e+1}} \int_{y_e}^{y_{e+1}} \left\{ D\, \underline{S}\left[\frac{\partial^4 \underline{S}}{\partial x^4} + 2\mu\frac{\partial^4 \underline{S}}{\partial x^2 \partial y^2} + \frac{\partial^4 \underline{S}}{\partial y^4} + 2(1-\mu)\frac{\partial^4 \underline{S}}{\partial x^2 \partial y^2}\right.\right.\right.$$

$$\left.\left.\left. - \rho h \omega^2 \underline{S}\,\underline{S}\, dx\, dy\right)\right\} \underline{W}^e = \underline{0} \qquad (3.10.b)$$

Integrating by parts, the partial differential equation reduces to

$$\underline{\underline{K}}^e \underline{W}^e - \lambda \underline{\underline{M}}^e \underline{W}^e = \underline{R}^e \qquad (3.10.c)$$

where $\underline{\underline{K}}^e$, $\underline{\underline{M}}^e$ and $\underline{R}^e$ are element stiffness matrix, element mass matrix and element stress-resultant vector and are given by

$$\underline{\underline{K}}^e = D \int_{x_e}^{x_{e+1}} \int_{y_e}^{y_{e+1}} \{(1-\mu)(\nabla\nabla \underline{S}).(\nabla\nabla \underline{S}) + \mu (\nabla^2 \underline{S})(\nabla^2 \underline{S})\} \, dx \, dy$$

$$= D \iint \left\{ \frac{\partial^2 \underline{S}}{\partial x^2} \frac{\partial^2 \underline{S}}{\partial x^2} + \mu \frac{\partial^2 \underline{S}}{\partial x^2} \frac{\partial^2 \underline{S}}{\partial y^2} + \mu \frac{\partial^2 \underline{S}}{\partial y^2} \frac{\partial^2 \underline{S}}{\partial x^2} + \frac{\partial^2 \underline{S}}{\partial y^2} \frac{\partial^2 \underline{S}}{\partial y^2} \right.$$

$$\left. + 2(1-\mu) \frac{\partial^2 \underline{S}}{\partial x \partial y} \frac{\partial^2 \underline{S}}{\partial x \partial y} \right\} dx \, dy \qquad (3.10.d)$$

$$\underline{\underline{M}}^e = \rho h \iint \underline{S} \, \underline{S} \, dx \, dy \qquad (3.10.e)$$

$$\underline{R}^e = D \int_{y_e}^{y_{e+1}} \left[\underline{S}\left(\frac{\partial^3}{\partial x^3} + \frac{\partial^3}{\partial x \partial y^2}\right)(\underline{S}.\underline{W}^e) - \frac{\partial \underline{S}}{\partial x}\left(\frac{\partial^2}{\partial x^2} + \mu \frac{\partial^2}{\partial y^2}\right)(\underline{S}.\underline{W}^e) \right.$$

$$\left. - (1-\mu) \frac{\partial \underline{S}}{\partial y} \frac{\partial^2}{\partial x \partial y} (\underline{S}.\underline{W}^e) \right]_{x_e}^{x_{e+1}} dy$$

$$+ D \int_{x_e}^{x_{e+1}} \left[\underline{S}\left(\frac{\partial^3}{\partial y^3} + \frac{\partial^3}{\partial y \partial x^2}\right)(\underline{S}.\underline{W}^e) - \frac{\partial \underline{S}}{\partial y}\left(\frac{\partial^2}{\partial y^2} + \mu \frac{\partial^2}{\partial x^2}\right)(\underline{S}.\underline{W}^e) \right.$$

$$\left. - (1-\mu) \frac{\partial \underline{S}}{\partial x} \frac{\partial^2}{\partial x \partial y} (\underline{S}.\underline{W}^e) \right]_{y_e}^{y_{e+1}} dx \qquad (3.10.f)$$

The element stiffness matrix and element mass-matrix are computed invoking Gauss-quadrature formula.

$$\int_{-1}^{1}\int_{-1}^{1} f(x, y)\, dx\, dy = \sum_{i=1}^{ngx}\sum_{j=1}^{ngy} w_i w_j\, f(x_i, y_j) \qquad (3.11)$$

in which w_i's are weight functions corresponding to the Gauss points (x_i, y_j), ngx and ngy being numbers of Gauss points along x-direction and y-direction respectively. In order to have the limits of integration -1 to 1 as indicated in equation (3.11), one transforms the variables in (3.10.a) and (3.10.b) into natural co-ordinates using the transformation given by equation (3.6). From this transformation, one obtains

$$\begin{aligned} dx\, dy &= pq\, d\xi\, d\eta, \\ \frac{\partial^2}{\partial x^2} &= \frac{1}{p^2}\frac{\partial^2}{\partial \xi^2} \\ \frac{\partial^2}{\partial y^2} &= \frac{1}{q^2}\frac{\partial^2}{\partial \eta^2} \end{aligned} \qquad (3.12)$$

and

$$\frac{\partial^2}{\partial x\, \partial y} = \frac{1}{pq}\frac{\partial^2}{\partial \xi \partial \eta}$$

Therefore, the element stiffness matrix and element mass matrix are obtained as

$$K_{ij}^{e} = D \int_{-1}^{1}\int_{-1}^{1} \left\{ \frac{q}{p^3}\frac{\partial^2 \phi_i}{\partial \xi^2}\frac{\partial^2 \phi_j}{\partial \xi^2} + \frac{\mu}{pq}\frac{\partial^2 \phi_i}{\partial \xi^2}\frac{\partial^2 \phi_j}{\partial \eta^2} + \frac{\mu}{pq}\frac{\partial^2 \phi_i}{\partial \eta^2}\frac{\partial^2 \phi_j}{\partial \xi^2} + \frac{p}{q^3}\frac{\partial^2 \phi_i}{\partial \eta^2}\frac{\partial^2 \phi_j}{\partial \eta^2} + \frac{2(1-\mu)}{pq}\frac{\partial^2 \phi_i}{\partial \xi \partial \eta}\frac{\partial^2 \phi_j}{\partial \xi \partial \eta} \right\} d\xi\, d\eta \qquad (3.12.a)$$

and

$$M^{e}_{ij} = \rho h \, pq \int_{-1}^{1} \int_{-1}^{1} \phi_i \phi_j \, d\xi \, d\eta \qquad (3.12.b)$$

As the limits of integrations in the equations (3.12.a) and (3.12.b) are in accordance with those in the equation (3.11), the integrations can be evaluated by Gauss-quadrature formula. The element stiffness matrix and mass matrix, are symmetric positive definite and are of the order 16 x 16. The element matrices of all the elements are assembled according to the standard procedure leading to the global stiffness and mass matrices which are partitioned after specifying the essential and the implied geometric boundary conditions from equation (3.5.a) so as to obtain an eigen-value problem

$$\left[\underline{\underline{K}} - \lambda \, \underline{\underline{M}} \right] \underline{W} = \underline{0} \qquad (3.13.a)$$

To solve this system, i.e. to obtain eigen-values and eigen-vectors, the NAG subroutine titled F02AEF is used. Its details have been discussed in Chapter 2. As in the case of the beam, here also the inverse eigen-value problem is solved considering the system of equations to be

$$\left[\underline{\underline{M}} - \mu \, \underline{\underline{K}} \right] \underline{W} = \underline{0} \qquad \text{where} \qquad \mu = \frac{1}{\lambda} \qquad (3.13.b)$$

3.4 DATA AND RESULTS:

The results have been obtained for the blade considered in reference [17]. The data is as follows:

$h = 0.025$ m

$\mu = 0.3$

$E = 200.0$ GPa

$\rho = 7800.0$ kg/m^3

For this data, the non-dimensionalised frequencies given by

$$\omega_o = \omega l^2 \left(\frac{\rho h}{D}\right)^{1/2} \qquad (3.14)$$

are computed for four different geometries. The first eight non-dimensionalised frequencies corresponding to each of the four geometries are given in the Table 3.1 below.

Table 3.1

Frequencies of the plate

Geometry		Non-dimensionalised frequency ω_o							
		I	II	III	IV	V	VI	VII	VIII
$\frac{l}{b}$	$\frac{b}{h}$	Y-Y bending	Torsion	X-X bending	Torsion	Y-Y bending	Torsion	Torsion	Y-Y bending
1	5	3.641	8.925	22.336	23.539	32.498	56.944	64.469	67.467
1	20	3.641	8.925	22.336	23.539	32.498	56.944	64.469	67.467
3	5	3.593	22.199	22.435	63.204	69.750	125.267	125.416	197.532
3	20	3.593	22.199	22.435	63.204	69.750	125.267	125.416	197.532

Note that these results are computed after the discretization of the plate in 25 equal elements with 36 total number

of nodes. The results are fairly close to those given in the reference [17] but do not exactly tally with it because the convergence of the frequencies with the increase in the number of elements is comparatively slow in this case and hence it requires more number of elements to acquire the desired accuracy. The increase in the number of elements is not possible owing to the limitations of the computer memory space required to store five square matrices and a few arrays. Needless to say, more accurate results cannot be obtained.

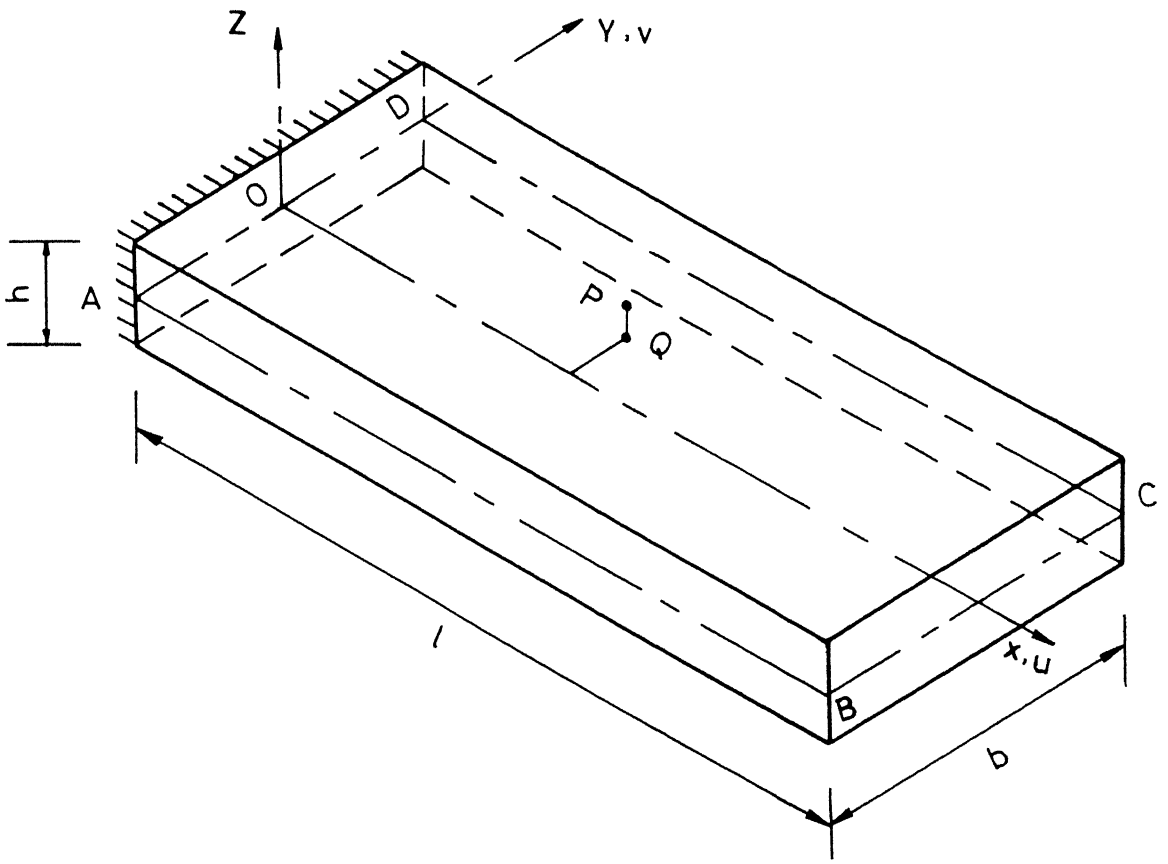

ABCD ≡ Neutral plane

Q ≡ (x, y, o) P ≡ (x, y, z)

w = displacement of Q

u, v = displacements of P

along x and Y directions.

FIG. 3.1 FLAT PLATE

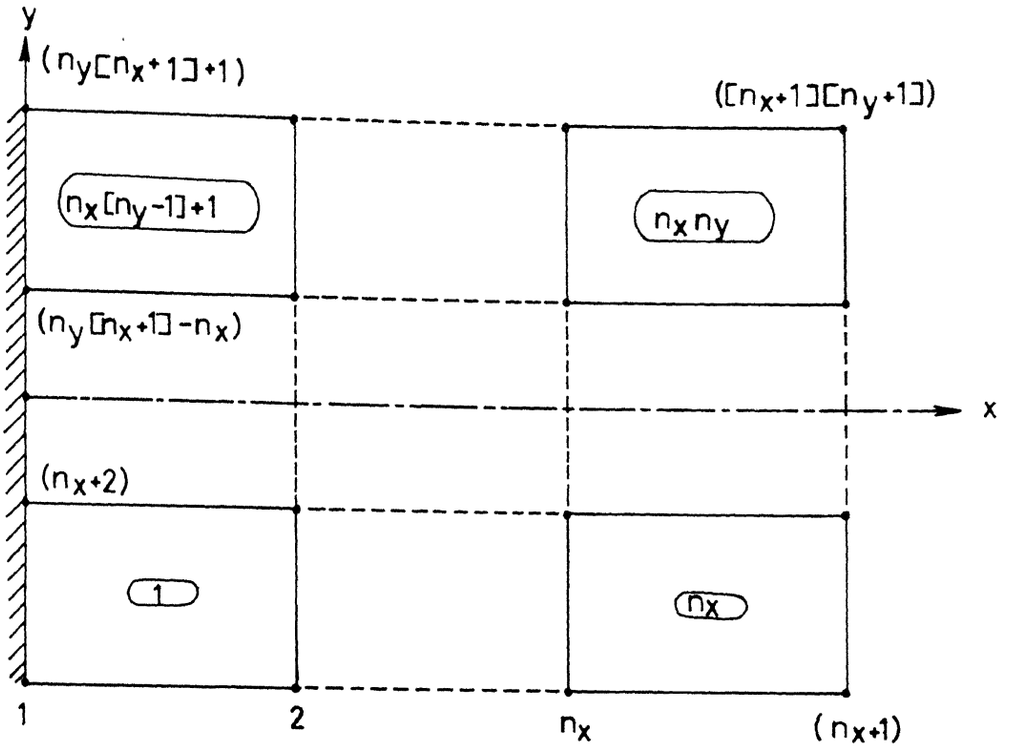

n_x = number of elements in the x direction
n_y = number of elements in the y direction
N.B. The encircled numbers represent the element numbers

FIG. 3.2.a DISCRETIZATION OF A CANTILEVER PLATE INTO A FINITE NUMBER OF FOUR-NODED ELEMENTS

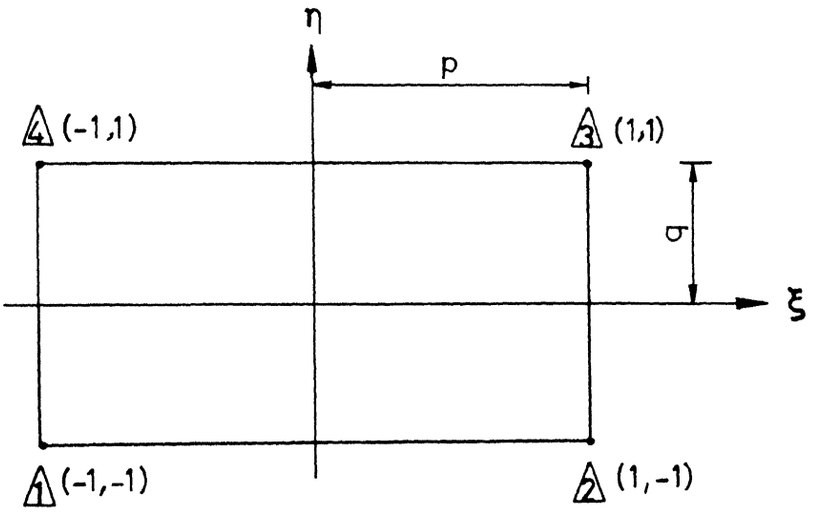

p, q - half the element length and breadth, respectively.

N.B. The numbers inscribed in the triangle respresent local node numbers

FIG.3.2.b A TYPICAL FOUR-NODED PLATE ELEMENT

CHAPTER 4

CONCLUSION

4.1 BLADE AS A BEAM:

Table 2.1 shows the natural frequencies corresponding to the coupled bending-bending-torsion modes of a long ($\frac{l}{b}$ = 5.53606), untwisted, cantilever beam of asymmetric aerofoil cross-section. The results are in agreement with analytical results of the reference [12].

Table 2.2 shows the natural frequencies corresponding to the coupled bending-bending modes and uncoupled torsional modes of a long ($\frac{l}{b}$ = 12), pre-twisted and cantilever beam of the rectangular cross-section. The results are in agreement with those in the reference [18]. The frequencies corresponding to flapwise bending and torsion increase with the increase in the angle-of-pre-twist while those corresponding to chordwise bending decrease. This is consistent with our expectations, as the area moment of inertia about X-X and the product of inertia of the section increase, the stiffness due to pre-twist and the effect of fibre-bending increase while the area moment of inertia about Y-Y decreases.

Table 2.3 also shows the results for a long beam ($\frac{l}{b}$ = 12) and there is a definite trend as far as the variation of the frequency with respect to the pre-twist is considered.

On the other hand, the results of Table 2.4 are for a short beam ($\frac{l}{b}$ = 1 or 3). Here some torsional or flapwise

bending frequencies decrease, chordwise bending frequencies increase while some frequencies do not exhibit any definite trend. This leads to the conclusion that

(i) Long blades can be analysed sufficiently accurately using a beam theory but not the short blades.

(ii) For long blades there seems to be a definite trend for the variation of frequency with respect to pre-twist.

4.2 BLADE AS A PLATE:

Table 3.1 shows the natural frequencies of a short blade for various length to breadth and breadth to thickness ratios. These frequencies are fairly close to those given in the reference [17]. It is observed that the frequencies for the same $\frac{l}{b}$ ratio are the same irrespective of the $\frac{b}{h}$ ratio. One can, therefore, draw the inference that

(i) Short flat blades can be analysed satisfactorily using the plate theory, and

(ii) The frequencies of short blades are independent of $\frac{b}{h}$ ratio as long as it is sufficiently small.

REFERENCES

1. HOUBOLT JOHN C. and BROOKS GEORGE W.,
"Differential equations of motion for combined flapwise bending, chordwise bending and torsion of twisted non-uniform rotor blades",
NACA Technical Notes, 1956.

2. CARNEGIE W.,
"Vibrations of pre-twisted cantilever blading: An additional effect due to torsion",
Proceedings of the Institution of Mechanical Engineers, pp. 315-322, Vol. 176, No. 13, 1962.

3. PARANJPE PRAMOD A.,
"Self-excited vibrations of turbomachine blading",
Journal of Applied Mathematics and Physics (ZAMP), pp. 598-608, Vol. 14, Fasc 6, 1963.

4. CARNEGIE W.,
"The application of the variational method to derive the equations of motion of vibrating cantilever blading under rotation",
Bulletin of Mechanical Engineering Education,
Pergamon Press, pp. 29-38, Vol. 6, 1967.

5. DUGGAN A.P. and SLYPER H.A.,
"Torsional vibrations of pretwisted cantilever beams",
International Journal of Mechanical Science,
Pergamon Press, pp. 871-883, Vol. 11, 1969.

6. BELGAUMKAR B.M., CARNEGIE W. and RAO J.S.,
"Torsional vibration of a cantilever beam of rectangular cross-section with uniform taper",
Bulletin of Mechanical Engineering Education,
Pergamon Press, pp. 61-67, Vol. 9, 1970.

7. CARNEGIE W. and RAO J.S.,
"Solution of the equations of motion of coupled-bending-bending torsion vibrations of turbine blades by the method of Ritz-Galerkin",
International Journal of Mechanical Science,
Pergamon Press, pp. 875-882, Vol. 12, 1970.

8. RAO J.S.,
"Flexural vibration of pre-twisted beams of rectangular cross-section",
Journal of the Aeronautical Society of India,
pp. 62-64, Vol. 23, No. 1, February 1971.

9. RAO J.S.,
"Coupled bending bending torsion vibrations of cantilever beams",
Journal of the Aeronautical Society of India,
pp. 265-268, Vol. 24, No. 1, February 1972.

10. RAO J.S.,
"Torsional vibrations of pre-twisted cantilever beams",
Journal of the Institution of Engineers (India),
pp. 211-212, Vol. 52, No. 9, Pt. CI5, May 1972.

11. CARNEGIE W. and RAO J.S.,
"Torsional vibration of pre-twisted tapered cantilever beams treated by collocation method",
Indian Journal of Pure and Applied Physics,
pp. 459-462, Vol. 10, June 1972.

12. RAO J.S.,
"Coupled vibrations of turbomachine blades",
Shock and Vibration Bulletin,
pp. 107-125, Bull. 47, Part 2, September 1977.

13. GUPTA R.S. and RAO S.S.,
"Finite element eigenvalue analysis of tapered and twisted Timoshenko beams",
Journal of Sound and Vibration,
pp. 187-200, Vol. 56, 1978.

14. BAJAJ G.R. and DHOOPAR B.L.,
"Free vibrations of packetted blades — coupled bending torsion modes",
pp. 123-135.

15. KULKARNI S.V., RAO J.S. and SUBRAHMANYAM K.B.,
"Coupled bending-bending vibrations of pre-twisted cantilever blading allowing for shear deflection and rotary inertia by the Reissner method",
International Journal of Mechanical Science,
Pergamon Press, pp. 517-530, Vol. 23, No. 9, 1981.

16. KAZA K.R.V. and SUBRAHMANYAM K.B.,
"Vibration analysis of rotating turbomachinery blades by an improved finite difference method",
International Journal for Numerical Methods in Engineering,
pp. 1871-1886, Vol. 21, 1985.

17. KIELB R.E., LEISSA A.W. and MACBAIN J.C.,
"Vibrations of twisted cantilever plates — A comparison of theoretical results",
International Journal for Numerical Methods in Engineering,
pp. 1365-1380, Vol. 21, Nol 8, August 1985.

18. SAURABH KUMAR,
"Coupled vibrations of turbine blades by finite element method",
M.Tech. Thesis, IIT KANPUR, 1982.

19. TIMOSHENKO S.P. and GOODIER J.N.,
"Theory of Elasticity",
McGraw Hill Book Co. - Singapore, Third edition, 1982.

20. TIMOSHENKO S.P.,
"Strength of materials, Part II: Advanced theory and problems",
D. Van Nostrand Co., Inc., Third edition, 1956.

21. TIMOSHENKO S.P. and WIONOWSKY-KRIEGER S.,
"Theory of Plates and Shells",
McGraw Hill Book Co., Singapore, Second edition, 1970.

22. BROCK A.E. and HOUGHTON E.L.,
"Aerodynamics for Engineering Students",
Edward Arnold (Publishers) Ltd., 1970.

23. CHURCH EDWIN F. JR.,
"Steam Turbines",
McGraw Hill Book Co., Inc., Third edition, 1950.

24. LEE JOHN F.,
"Theory and Design of Steam and Gas Turbines",
McGraw Hill Book Co., Inc., 1954.

25. SCHWARZ H.R., RUTISHAUSER H. and STIEFEL E.,
"Numerical Analysis of Symmetric Matrices",
Prentice-Hall, Inc., 1973.

26. SOEDEL W.,
"Vibrations of Shells and Plates",
Marcel Dekkar Inc., 1981.

27. BREBBIA C.A. and CONNOR J.J.,
"Fundamentals of Finite Element Techniques",
John Wiley and Sons, New York-Toronto, 1974.

28. COOK R.D.
"Concepts and Applications of Finite Element Analysis",
John Wiley and Sons, Inc., Second edition, 1981.

29. ZIENCIWICZ O.C.
"The Finite Element Method",
Tata McGraw Hill Book Co. Ltd., 1979.

30. NAG MARK 10 User's Manual.

APPENDIX I

THE ZUKOVSKY TRANSFORMATION 22

The Zukovsky transformation 22

$$\zeta = z + \frac{q^2}{z} \quad \text{where} \quad z = x + iy \quad \text{and} \quad \zeta = \xi + i\eta \qquad (I.1)$$

is a conformal mapping that transforms a circle in the z-plane into an aerofoil section in the ζ-plane as shown in the Figure 2.3.

For any point p on the circle in the z plane,

$$r = q\ e\cos\theta + s\sin\theta + t\cos\gamma \qquad (I.2)$$

For small values of e and ,

$$\left(\frac{r}{q} + \frac{q}{r}\right) \quad 2 \quad \text{and}$$

$$\left(\frac{r}{q} - \frac{q}{r}\right) \quad 2\theta(1 + \cos\theta) + 2\beta\sin\theta \qquad (I.3)$$

Substituting $z = r\ e^{i\theta}$ in the Zukovsky transformation, one gets

$$\xi = 2q\cos\theta \quad \text{and}$$

$$\eta = 2q\ e(1 + \cos\theta)\sin\theta + 2q\beta\sin^2\theta \qquad (I.4)$$

Using (I.4), the thickness, the area, the area moments of inertia and the product of inertia can be obtained as:

$$h = 4q\ e\sin\theta(1 + \cos\theta)$$

$$A = 4\pi q^2 e$$

$$I_{\xi\xi} = 2\pi q^4 e(3e^2 + 5\beta^2)$$

$$I_{\eta\eta} = 4\pi q^4 e \qquad \text{(I.5)}$$

$$I_{\xi\eta} = 2\pi q^4 e \beta$$

when β is very small compared to e, the inclination of the principal axes 1 and 2 with respect to the $\xi - \eta$ axes is quite small, usually of the order of 2°. Then

$$I_{11} \simeq \lim_{\beta \to 0} I_{\xi\xi} = 6\pi q^4 e^3$$

$$I_{22} \simeq \lim_{\beta \to 0} I_{\eta\eta} = 4\pi q^4 e \qquad \text{(I.6)}$$

For this case , the expression for q and e are

$$q = (I_{22}/A)^{1/2}, \qquad e = (2I_{11}/3I_{22})^{1/2} \qquad \text{(I.7)}$$

The chord length of the blade comes out to be

$$b = 4q = 4(I_{22}/A)^{1/2} \qquad \text{(I.8)}$$

The maximum thickness is obtained by maximising the expression h_ξ of equation (I.5):

$$h = 3\sqrt{3}\, q\, e = 3(2I_{11}/A)^{1/2} \qquad \text{(I.9)}$$

APPENDIX II

HOUSEHOLDER'S DECOMPOSITION

Normally a non-singular symmetric matrix P is decomposed as

$$[P] = [U]^T [Q] [U] \qquad \text{(II.1)}$$

where $[U]$ is orthogonal and $[Q]$ is positive definite. However, instead of expressing this transformation as a product involving two matrices, one can express it in terms of a matrix and a column vector by expressing $[U]$ as

$$[U] = [I] - 2\{W\}\{W\}^T \qquad \text{(II.2)}$$

where W is a normalised column vector.

It can be found out by the relation

$$W_1 = 0,$$

$$W_2 = \left[\frac{1}{2}\left(1 \mp \frac{P_{12}}{s}\right)\right]^{1/2}$$

$$W_k = \mp \frac{P_{1k}}{2s\,W_2} \qquad \text{for } k = 3, 4 \ldots n$$

where

$$s = P_{1i}\,P_{1j}(1 - \delta_{ij}) \qquad \text{(II.3)}$$

and the sign in the expression for W_2 and W_k can be chosen to be that of P_{12}.

Using (II.1) and (II.2) the decomposition for P can be expressed as

$$[P] = [Q] - 2\{W\}\{W\}^T[Q] - 2[Q]\{W\}\{W\}^T + 4\{W\}\{W\}^T[Q]\{W\}\{W\}^T \qquad \text{(II.4)}$$

Advantages:

i) For the higher order matrix P , less computer memory locations are required as in lieu of a matrix U of the order n x n, a column vector W of n components is utilized.

ii) Computational economy and numerical accuracy can be achieved simultaneously.